Doctoral Thesis

Towards a microscopic description of nuclear reactions: Time dependent generator coordinate method for many particle tunneling

(核反応の微視的記述に向けて:
多粒子系のトンネル効果に対する
時間依存生成座標法の開発)

Naoto Hasegawa

Depertment of Physics
Graduate School of Science
Tohoku University

2021

Abstract

Nuclear fusion is a process in which two nuclei collide to form a larger nucleus. Nuclear fusion can be divided into three stages. First, the two nuclei contact each other across the potential barrier (the Coulomb barrier) created by the nuclear force and the Coulomb interaction between the two nuclei. Next, the energy of the relative motion of the two nuclei at the time of the collision is converted into energy for the internal excitations, and then the relative motion is trapped inside the Coulomb barrier. Finally, if the compound nucleus is de-excited by particle emissions to a nucleus in the ground state, it is called fusion-evaporation or if the compound nucleus fission back to two nuclei, it is called fusion-fission. Fusion reactions play an important role in many ways, including nucleosynthesis in stellar interiors and productions of superheavy nuclei.

The time-dependent Hartree-Fock (TDHF) method has been widely used as a theory to describe nuclear reactions, including nuclear fusion. This method is based on the mean-field approximation to the solution of the many-body Schrödinger equation, which is usually too complicated to solve. The TDHF enables one to describe nuclear reactions in terms of nucleon degrees of freedom. By describing reactions using nucleon degrees of freedom, we can automatically take into account a variety of internal excitations during a reaction process. TDHF has been successfully applied to a wide range of phenomena, including heavy-ion reactions, such as nucleon transfer [1–4], quasifission [5–8], induced fission [9–11], and fusion [12–17].

On the other hand, the TDHF is known to have some drawbacks. In TDHF, quantum fluctuations are drastically underestimated [101], and thus quantum tunneling, a fundamental phenomenon in quantum mechanics, cannot be fully described. Therefore, this method is applicable only to reactions at energies above the Coulomb barrier. In reality, there are sub-barrier fusions that occur at energies lower than the Coulomb barrier, which is caused only by the quantum tunneling effect. This cannot be described in the TDHF framework. Note that almost all fusion reactions in stellar interiors are sub-barrier fusion.

Although several extensions of TDHF have been considered to overcome these drawbacks, no method has yet been developed that can include both the various internal excitations and the tunneling effect, two necessary aspects of sub-barrier fusion.

In order to overcome the lack of a suitable method for describing sub-barrier fusions, in this thesis, we have developed a theory that includes both internal excitations and tunneling effect based on the idea of the Time-Dependent Generator Coordinate Method (TDGCM). In TDGCM, the time-dependent Slater determinants are superposed with time-dependent weights. The TDGCM describes the tunneling effect by using the Slater determinant which in a sense behaves classically. We have first applied the TDGCM to a collision of two ^{4}He particles in one-dimension, and qualitatively confirmed that the TDGCM can describe the tunneling effect. We have also argued that the TDGCM describes the tunneling effect by exchanging energy between superposed Slater determinants. Next, we have applied the TDGCM to a collision of a ^{4}He particle on an external barrier in one-dimension and calculated the collision-energy dependence of the transmission probability. As a result, we have obtained finite tunneling probabilities at sub-barrier energies which cannot be described [37] in TDHF. We have also confirmed that the collision energy dependence of the transmission probability calculated by TDGCM is not 0 or 1 as obtained by TDHF but becomes a smooth function of energy. As the last calculation, TDGCM has been applied to the collision of two ^{4}He particles in three-dimensions. The result showed that TDGCM can describe the tunneling effect in three-dimension as well as in one-dimension. This is important because it is necessary to work in three-dimension when TDGCM is applied to realistic calculations.

In our research, TDGCM was applied only to simple systems, but TDGCM is expected to have a similar or even a larger application range than TDHF. In addition, TDGCM can describe nuclear reactions with sub-barrier energies, which cannot be described by existing methods such as TDHF. In particular, nuclear reactions with sub-barrier energies in difficult experimental regions, such as superheavy-element synthesis and neutron-rich nuclei, can be described only by TDGCM, which is a microscopic theory with little dependence on experiments and can also describe tunneling effect. In our research, we have only developed the basis of TDGCM. However the construction of this theory would be a big step to solve the problem of tunneling effect, which has been unsolved for decades since the invention of TDHF, and to expand the range of application of microscopic theory.

Acknowledgement

First of all, I would like to express my utmost gratitude to my supervisor, Prof. Kouichi Hagino, for all the help he has given me with my research and thesis writing. He has guided my research for five years, starting when I was a master's student. Without his help, I would not have been able to complete my research and this doctoral thesis.

I would also like to express my gratitude to Prof. Yusuke Tanimura, who has always been close to the students and has helped me with discussions and given me advice. He helped me with everything from research consultations to English editing.

I would like to thank Prof. Shoichi Sasaki, Prof. Emiko Hiyama, Prof. Akira Ono, Prof. Shimpei Endo, and Prof. Hajime Togashi for their valuable advice in group seminars and discussions.

I would like to thank Dr. Denis Lacroix for the many discussions we had during my visit to France, and for the useful advice he gave me on my future research plans.

I would like to thank Prof. Haozhao Liang for the informative discussion on systems with exact solutions where TDGCM can be applied.

I would like to thank Prof. Kazuyuki Sekizawa, Prof. Jørgen Randrup, and Prof. Akira Onishi for the useful discussions we had.

I would like to thank the students in my laboratory and the graduating seniors for their discussions, which also helped me with my research.

Finally, I would like to thank my family for allowing me to study at Tohoku University until my doctoral course and for their continuous support.

This work was supported by the Tohoku University Graduate Program on Physics for the Universe (GP-PU), and JST SPRING, Grant Number JPMJSP2114.

Contents

Chapter 1

Introduction

1.1 Overview of Nuclear Reactions

1.1.1 Nuclear systems

An atomic nucleus is a quantum many-body system consisting of protons and neutrons. The number of nucleons that make up a nucleus can range from a few to about 250. There are the nuclear force, which is a short-range attractive force between nucleons, and the Coulomb force, which is a long-range repulsive force between protons.

The variety of phenomena caused by nuclei is not limited to the field of atomic nuclei, but is also important for other fields such as astrophysics. For example, elemental synthesis [27], which is the search for the origin of matter, requires knowledge of many nuclear phenomena, such as nuclear fusion [12–17, 26], fission [5–11, 18–20, 23, 47, 50, 52, 71, 72], neutron-rich nuclei [28, 29], and nucleon transfer reactions [1–4, 101].

However, dealing with atomic nuclei is also challenging. One of the difficulties in dealing with nuclei is that the number of nucleons is halfway. In other words, the number of nucleons in most nuclei is neither small enough to be treated rigorously, nor large enough to be treated statistically. The fact that the nuclear force is not completely understood [32] is another difficulty in dealing with nuclei. There are still many attempts to consider three-body [30, 31] or more interactions and to derive the nuclear force from QCD [33].

How to overcome these difficulties and describe nuclear phenomena quantitatively is the goal of this field.

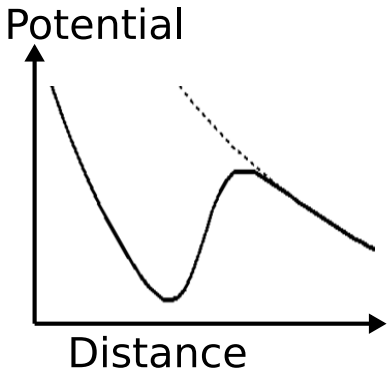

Figure 1.1: Schematic picture of internuclear potential as the function of distance between the two nuclei. Potential pocket and Coulomb barrier exist due to the nuclear force, which is a short-range force, and the Coulomb force, which is a long-range force.

1.1.2 Nuclear reactions

Recent hot topics in nuclear physics include superheavy nuclei and stellar nucleosynthesis. Heavy ion fusion reactions are important in these phenomena, where heavy ions are nuclei heavier than ^{4}He. Fusion reaction is a reaction in which two nuclei collide to form a single nucleus. The potential between two nuclei exists as a function of the distance between the nuclei due to the nuclear force (short-range attraction) and the Coulomb force (long-range repulsion), as shown in the Fig. 1.1. The potential barrier shown in this figure is called the Coulomb barrier. In the first stage of nuclear fusion, the relative motions between nuclei must approach beyond this Coulomb barrier. In the next stage, the energy of the relative motion of the nuclei is converted into the motion of the nucleons inside the nucleus, i.e., internal excitation, and the relative motion is trapped inside the Coulomb barrier to form an excited compound nucleus. As the last stage of fusion, the excited compound nucleus is de-excited mainly by neutron emission especially in light nuclei, and fusion is completed when it reaches the ground state. It should be noted that the actual process of fusion is not a straightforward one; sometimes the nucleus is reflected by the Coulomb barrier, and sometimes it fissions after the formation of the compound nucleus but before the de-excitation especially in heavy nuclei (this phenomenon is called fusion-fission).

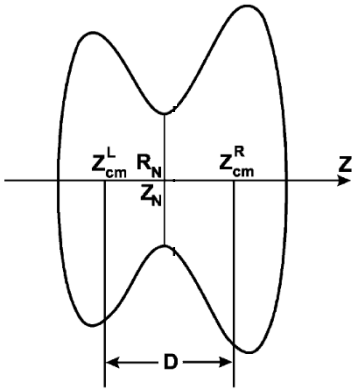

Figure 1.2: Schematic picture of a nucleus in a droplet model with several parameters. The $Z^{\mathrm{L}}_{\mathrm{cm}}$ and $Z^{\mathrm{R}}_{\mathrm{cm}}$ denote the positions of the mass centers of left and right fragments respectively. The Z_{N} and R_{N} are the coordinate of the minimum of neck thickness and its radius. D is the distance between $Z^{\mathrm{L}}_{\mathrm{cm}}$ and $Z^{\mathrm{R}}_{\mathrm{cm}}$. Sometimes, we also take the mass asymmetry of the left and right fragment as another parameter. This figure was taken from [18].

1.1.3 Theories for nuclear reactions

Theories for such nuclear reactions, including heavy-ion fusion, are classified into macroscopic and microscopic approaches. The macroscopic approach is an approach considering only effective collective motions that describe the phenomena of interest. Here, collective motions are coherent motions of many nucleons, such as the center-of-mass motion of a nucleus or the vibration of a nucleus as a whole. The advantages of the macroscopic approach are a reduced computational cost by limiting the degrees of freedom and the ease of intuitive understanding through modeling. On the other hand, the disadvantages of the macroscopic approach are the arbitrariness in the choice of degrees of freedom, and a need to adjust model parameters by fitting to experimental data and adding degrees of freedom to match the experimental results for the system or phenomenon of interest.

An example of modeling a phenomenon in a macroscopic approach is a droplet model [34]. In the droplet model, a nucleus is viewed as a classical droplet, and the collective degrees of freedom are selected from among its shapes (Fig. 1.2). The equations of motion for the selected degrees of freedom are often solved by taking into account the unselected degrees of freedom using the Langevin method. In the Langevin method, the unchosen degrees of freedom are considered as heat bath, and the energy exchange with them is incorporated as dissipation to the heat bath and a random

force from the heat bath. Another example of a macroscopic approach is the coupled-channels method [35, 36] using collective degrees of freedom. This method solves the two-body problem of two nuclei while incorporating collective excitations in those nuclei. For example, one can choose the distance between nuclei, the deformation of one nucleus, and the angle relative to the other nucleus as dynamical degrees of freedom. Then the "coupled channels equation" is obtained, which is an equation of motion for the relative motion of two nuclei combining various angular momentum and vibrational excited states.

Despite these advantages, the macroscopic approach, which has an empirical aspect, is not suitable to describe reactions in unknown regions such as superheavy nuclei and neutron-rich nuclei, where experiments are difficult. The microscopic approach with only nucleon-nucleon interaction as input is advantageous for such a region. In the microscopic approach, once the nucleon-nucleus interaction is determined from the static properties of nuclei and experimental results of scattering, nuclear reactions can be described without free parameters. In other words, there is no need to adjust the parameters depending on the phenomenon of interest. In particular, some reactions in heavier than medium-heavy nuclei can be described by methods based on the mean-field approximation, such as the time-dependent Hartree-Fock method (TDHF) , although there are still problems shown below. The TDHF approximates the motion of an interacting fermion to that of an independent fermion with a self-consistent one-body potential, which allows us to approximate the solution of the many-body Schrodinger equation, which is usually impractical to solve. The TDHF has been used successfully in nucleon transfer reactions and nuclear fusion to describe their average features (See Chap. 2).

1.2 Difficulties in microscopic approach for reactions

Although TDHF has the advantages for the microscopic approach as described above, it also has some principle drawbacks. The quantum fluctuations of the collective motion calculated by TDHF are considerably underestimated, and quantum tunneling, which is a characteristic phenomenon in quantum mechanics, cannot be described properly. This is because the wave function of the TDHF is always localized in a self-consistent one-body potential, and the wave packet transmitted through the barrier and the wave packet reflected by the barrier cannot be represented simultaneously. This

drawback can be fatal in describing nuclear reactions, especially nuclear fusions at energies below the Coulomb barrier, which occur only with quantum tunneling. Such reactions cannot be described at present.

Various methods have already been considered to solve this problem in microscopic approaches. An example is the Stochastic Mean-Field (SMF) [56, 58, 59, 92–94], which considers the wave functions calculated by TDHF with different initial values as a statistical population and calculates the quantum fluctuation as a statistical fluctuation. Another example includes the simplified Time-Dependent Generator Coordinate Method (simplified TDGCM) [21], proposed by Reinhard in 1983, which recovers quantum fluctuations by superposing the TDHF wave functions and changing the weights of each wave function with time. These methods have been applied to nucleon transfer reactions and nuclear oscillations, and the results show larger quantum fluctuations than TDHF. Since these methods are based on the time-dependent TDHF wave function, they inherit the advantage of TDHF in that internal excitations are automatically taken into account, but on the other hand, they still have the disadvantage that they cannot describe quantum tunneling phenomena. An extension that can describe quantum tunneling phenomena is being considered, such as the Time-Dependent Hill-Wheeler (TDHW) [19, 20, 70–72] method, which has been applied to fission and other applications in the last decade. The TDHW describes the quantum tunneling effect by superposing states prepared by the time-independent Hartree-Fock method and varying their weights with time. By initially preparing the Hartree-Fock states before, during, and after the barrier penetration, the penetration through the barrier can be expressed by the transition of the weights on the states, and as a result, the quantum tunneling phenomenon can be described. However, this method is based on the time-independent Hartree-Fock method, and cannot automatically incorporate the internal excitations of nuclei, so it cannot be called a complete microscopic method, but rather a macroscopic method that uses the microscopic method as input. These extensions, especially TDHW and simplified TDGCM, will be discussed in detail in Chap. 2.

1.3 Aims of this work

To summarize the problems with the microscopic approach described above, it has not yet been established that the microscopic approach can automatically incorporate the internal excitations of nuclei and describe the quantum tunneling phenomenon. This problem is particularly critical for low-energy fusion, because fusion involves a variety of internal excitations, and fusion at

sub-barrier energies is always accompanied by quantum tunneling. Therefore, we have developed a method to simultaneously describe internal excitations and quantum tunneling by extending Reinhard's TDGCM to describe low-energy fusion reactions.

In the simplified TDGCM, the internal excitations are automatically incorporated by using a time-dependent Slater determinant, and the quantum fluctuations lost in the TDHF are recovered by superposing Slater determinants. However, it still fails to describe quantum tunneling because the Slater determinants, which are the basis for the superposition, are evolved in time with independent TDHF, and as a result, no basis could be prepared to describe quantum tunneling. In our TDGCM, the idea of superposing the time-dependent Slater determinant is retained, but the correlation between the time-dependent Slater determinants are considered, which was not considered in the simplified TDGCM. With this improvement, bases across the barrier can be prepared, and the quantum tunneling effect can be described more efficiently.

In this thesis, we first construct the TDGCM and derive the equations of motion for nucleons. Then we apply it to three simple systems, and demonstrate that TDGCM can describe tunneling. We also discuss how well it can describe tunneling probability, and whether it can be applied to realistic calculations in a future.

The thesis is organized as follows. First, in Chap. 2, we will explain in detail the TDHF, which is widely used as a microscopic theory of nuclear reactions. It also provides the basis of our TDGCM. We will list and explain some of the methods devised to overcome the shortcomings of the TDHF. We will compare them with our TDGCM. In Chap. 3, we will explain how and why TDGCM are able to describe internal excitations and quantum tunneling. In Chap. 4, we will discuss the properties of TDGCM through the application of TDGCM to three simple systems: the one-dimensional ^{4}He+^{4}He collision system, the one-dimensional collision of ^{4}He with an external barrier, and the three-dimensional ^{4}He+^{4}He collision system. In the last chapter, Chap. 5, we will summarize this work and discuss future perspectives.

Chapter 2

Review of existing theories

TDHF is one of the most widely used microscopic methods for nuclear reactions. Since TDHF is a microscopic method that treats the nucleon degrees of freedom as they are, it can automatically incorporate the internal excitations of nuclei. On the other hand, TDHF has a disadvantage that the TDHF considerably underestimates the quantum fluctuation of the collective motion (e.g., the center-of-mass motion and oscillation of nuclei) and cannot describe the quantum tunneling phenomenon. In this chapter, the characteristics of TDHF are discussed by deriving the equation of motion of the wave function in TDHF, and actual successful and unsuccessful cases of TDHF are shown. After the introduction of TDHF, we will introduce methods beyond TDHF, such as the Time-Dependent Hill-Wheeler method (TDHW) [19, 20, 70–72] and the simplified Time-Dependent Generator Coordinate Method (simplified TDGCM) [21].

2.1 Time-Dependent Hartree-Fock

2.1.1 Derivation of the time-dependent Hartree-Fock equation

The concept of the TDHF is to approximate interacting fermions as independently moving fermions in a self-consistent one-body potential. In the following, we derive the TDHF equation, i.e., the equation of motion in the TDHF, based on this concept.

First, we define the one-body density matrix as follows

$$\rho_{kl}(t) = \langle \Psi(t) | c_l^\dagger c_k | \Psi(t) \rangle \,, \tag{2.1}$$

where $c^\dagger, c$ are the nucleon creation and annihilation operators, respectively, and the subscripts k and l are the labels of the single-particle state of the

nucleon. By differentiating this density matrix with respect to time, the time-evolution equation of the density matrix is obtained as follows

$$i\hbar\dot{\rho}_{kl}(t) = \langle\Psi(t)|[c_l^\dagger c_k, H]|\Psi(t)\rangle\,, \tag{2.2}$$

where H is the Hamiltonian, and we have used the fact that the time evolution of a state can in general be written in terms of H as follows

$$|\Psi(t)\rangle = e^{-\frac{iHt}{\hbar}}\,|\Psi(0)\rangle\,. \tag{2.3}$$

Here, the Hamiltonian is assumed to be in the following form considering up to a two-body interaction

$$H = \sum_{l_1 l_2} t_{l_1 l_2} c_{l_1}^\dagger c_{l_2} + \frac{1}{4}\sum_{l_1 l_2 l_3 l_4} \bar{v}_{l_1 l_2, l_3 l_4} c_{l_1}^\dagger c_{l_2}^\dagger c_{l_4} c_{l_3}, \tag{2.4}$$

$$\bar{v}_{l_1 l_2, l_3 l_4} = v_{l_1 l_2 l_3 l_4} - v_{l_1 l_2 l_4 l_3}, \tag{2.5}$$

where $\bar{v}$ in Eq. (2.5) is an antisymmetrized matrix element of the interaction v. By substituting this Hamiltonian into Eq. (2.2) and using the anti-commutation relation $\{c_i^\dagger, c_j\} = \delta_{ij}$, the following equation is obtained:

$$i\hbar\dot{\rho}_{kl} - \sum_p (t_{kp}\rho_{pl} - \rho_{kp}t_{pl}) = \frac{1}{2}\sum_{prs}(\bar{v}_{kprs}\rho^{(2)}_{rslp} - \bar{v}_{rslp}\rho^{(2)}_{kprs}). \tag{2.6}$$

Here, the two-body density matrix $\rho^{(2)}$ is defined as follows

$$\rho^{(2)}_{klpq}(t) = \langle\Psi(t)|c_p^\dagger c_q^\dagger c_l c_k|\Psi(t)\rangle\,. \tag{2.7}$$

The left-hand side of Eq. (2.6) describes the motion of a free particle. On the other hand, the right-hand side describes the dynamics of the interaction. The two-body density matrix on the right-hand side of Eq. (2.6) can be divided into two components from the Wick's theorem as follows

$$\rho^{(2)}_{klpq} = \rho_{kp}\rho_{lq} - \rho_{kq}\rho_{lp} + g^{(2)}_{klpq}. \tag{2.8}$$

The first and second terms on the right-hand side of Eq. (2.8) are the terms of the two-body density that can be expressed in terms of the one-body density, and the third term, defined by this decomposition is the two-body correlation. Eq. (2.6) can then be transformed as

$$i\hbar\dot{\rho}_{kl} - [t+\Gamma, \rho]_{kl} = \frac{1}{2}\sum_{prs}(\bar{v}_{kprs}g^{(2)}_{rslp} - \bar{v}_{rslp}g^{(2)}_{kprs}), \tag{2.9}$$

where the mean-field potential Γ is defined as

$$\Gamma_{kl} = \sum_{pq} \bar{v}_{kqlp}\rho_{pq}. \tag{2.10}$$

In the mean-field approximation, we ignore the right-hand side of Eq. (2.9). In other words, by ignoring $g^{(2)}$, the time evolution equation of the density in the mean-field approximation is obtained as

$$i\hbar\dot{\rho} = [h, \rho], \tag{2.11}$$

where we have set $t + \Gamma = h$.

Using the coordinate representation and ignoring the spin degrees of freedom, the one-body density matrix within Hartree-Fock approximation is given by the following equation using the single-particle wave function ϕ_i

$$\rho(\vec{r}, \vec{r}', t) = \sum_{i=1}^{A} \phi_i^*(\vec{r}, t)\phi_i(\vec{r}', t). \tag{2.12}$$

Using the density matrix Eq. (2.12) and considering the spin-independent two-body potential $v(\vec{r}, \vec{r}')$, Eq. (2.11) can be expressed for the single-particle wave function as follows

$$i\hbar\frac{\partial}{\partial t}\phi_i(\vec{r}, t) = \left(-\frac{\hbar^2}{2m}\Delta + \Gamma_H(\vec{r}, t)\right)\phi_i(\vec{r}, t) + \int d^3r'\Gamma_{\rm ex}(\vec{r}, \vec{r}', t)\phi_i(\vec{r}', t). \tag{2.13}$$

Here, the Hartree potential Γ_H and the exchange potential $\Gamma_{\rm ex}$ are defined as follows

$$\Gamma_H(\vec{r}) = \int d^3r' v(\vec{r}, \vec{r}') \sum_{j=1}^{A} |\phi_j(\vec{r}')|^2 = \int dr' v(\vec{r}, \vec{r}')\rho(\vec{r}'), \tag{2.14}$$

$$\Gamma_{\rm ex}(\vec{r}, \vec{r}') = -v(\vec{r}, \vec{r}') \sum_{j=1}^{A} \phi_j(\vec{r}')^*\phi_j(\vec{r}) = -v(\vec{r}, \vec{r}')\rho(\vec{r}, \vec{r}'). \tag{2.15}$$

Eqs. (2.13)-(2.15) give the time evolutions of the single-particle wave functions in the TDHF.

TDHF from a viewpoint of time-dependent variational principle

Note that this Eq. (2.13) can also be obtained by the time-dependent variational method (See Sec. 3.1). The time-dependent variational method is simply a method of finding an approximate solution to the Schrödinger equation

in a restricted Hilbert space, that uses the Lagrangian defined as follows

$$\mathcal{L} = \langle \Phi(t) | i\hbar \frac{\partial}{\partial t} - H | \Phi(t) \rangle \,. \tag{2.16}$$

Here, we will use the Slater determinant composed of the single-particle wave function for the trial function $|\Phi(t)\rangle$, and define the following action

$$A = \int_{t_1}^{t_2} \mathcal{L}[\phi, \phi^*] dt \tag{2.17}$$

where the variation at the end points are fixed $\delta\phi(t_{1,2}) = \delta\phi^*(t_{1,2}) = 0$. Then the condition that the variation of this action with respect to ϕ and ϕ^* is zero

$$\delta A = 0 \tag{2.18}$$

gives the equation of motion (2.13). This fact means that TDHF is equivalent to a time-dependent variational method with a restriction of the trial function to a Slater determinant.

TDHF features and application examples

To summarize the features of TDHF, the first thing to note is that TDHF uses an approximation that ignores the interactions that cannot be expressed in terms of one-body densities, such as those appearing in the right-hand side of Eq. (2.9). It also ignores effects such as direct nucleon collisions. However, a part of the two-body density that can be expressed as the product of the one-body density is incorporated. This can be seen as a partial incorporation of the effect of nucleon collisions due to those with the one-body potential and the correlation between nucleons through the one-body potential. In addition, Eq. (2.13) shows that the two potentials in the equation of motion of the nucleon in the TDHF are both functionals of the one-body density of the nucleus, which means that the nucleus is trapped in the one-body potential created by itself in the TDHF. This feature of TDHF, in which the wave function evolves in time while being trapped in this self-consistent one-body potential, causes the wave function to be always localized, leading to underestimation of quantum fluctuations and a failure to describe quantum tunneling phenomena because the wave function never splits into two wave packets.

We will now discuss some of the successes and failures of TDHF. First, a successful example is shown in Fig. 2.1. Fig. 2.1 shows the results of the

TDHF calculation for the ^{64}Ni+^{238}U reaction. The energy of the collision in the center-of-mass system is 307 MeV.

Panel (A) shows the production cross sections for various proton transfer channels (the number of transferred protons is shown in ±xp). Plus (minus) represents the transfer from ^{238}U to ^{64}Ni (and vice versa)) as a function of the mass number of the reaction product. The red dots are experimental data, histogram is the cross section of the primary product by TDHF and the blue histogram is the cross section of the secondary product by TDHF+GEMINI where GEMINI is a program that calculates particle evaporation by means of a statistical model. Also cross sections by the semiclassical model GRAZING6 are also shown for comparison. Neutron evaporation effects are also shown in green shaded histograms. It can be seen from this panel (A) that in many cases, THDF gives results closer to experimental results than the semi-classical method; the TDHF calculation combined with the GEMINI method for calculating nuclear de-excitation also gives results closer to experimental results. Panel (B) shows the time evolution of the density in the reaction plane. In peripheral collisions (impact parameter b = 5.5 fm), the multi-nucleon transfer process shown in (A) takes place. The elapsed time of the simulation is zeptoseconds (1zs = 10-21 s). TDHF calculates the time evolution of the nucleus and allows us to see the state of the nucleus at each time, as shown in this panel (B). Panel (C) shows the relationship between the total kinetic energy (TKE) and the outgoing fragment mass number A. The left panel (a) shows the TDHF calculation and the right panel (b) shows the experimental results. This comparison shows that the TDHF calculation is able to describe the average behavior of the experimental results, but at the same time it is not able to describe the quantum fluctuations. Panel (D) shows the same as panel (B), but with a smaller impact parameter (b = 2 fm), where the quasi-fission process shown in (C) occurs, where two nuclei are united by a collision and then split again. In the panel, x-, y-, and z- indicate the orientation of the deformed ^{238}U.

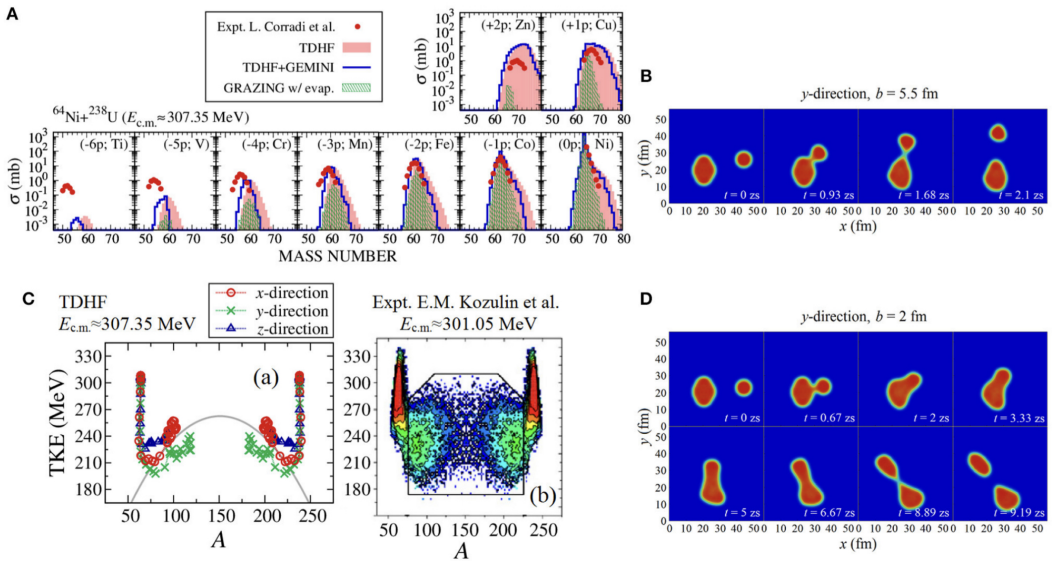

Figure 2.1: Results of TDHF calculations for the ^{64}Ni+^{238}U reaction at $E_{\rm c.m.} \simeq 307$ MeV (A) Production cross sections for various proton transfer channels [indicated by (±xp), where plus (minus) sign corresponds to transfer from ^{238}U to ^{64}Ni (vise versa)] as a function of the mass number of the reaction products. Red points are the experimental data [102], red-filled histograms are cross sections for primary products by TDHF [23], and blue histograms are cross sections for secondary products by TDHF+GEMINI [24]. For comparison, cross sections by a semi-classical model, GRAZING6 , including neutron evaporation effects, are also shown by green shaded histograms. (B) This picture exhibits the time evolution of the density in the reaction plane in a peripheral collision (b = 5.5 fm), where MNT processes shown in (A) take place. Elapsed time in the simulation is indicated in zeptoseconds (1 zs = 10^{-21} s). (C) Correlation between the total kinetic energy (TKE) and the mass number A of the outgoing fragments. The left figure (a) shows results of TDHF calculations [23], while the right figure (b) shows the experimental data [25]. (D) Same as (B), but for a smaller impact parameter (b = 2 fm), where quasi-fission processes shown in (C) take place. In the figure, x-, y-, and z-direction indicate the orientation of deformed ^{238}U [23]. In this way, TDHF can describe both peripheral and damped collisions in a unified way. This figure was taken from [101].

Next, we present a comparison between the experimentally observed and TDHF calculated fusion cross sections. Fig. 2.2 shows the fusion cross sections for ^{16}O+^{208}Pb as a function of collision energy in the center-of-mass

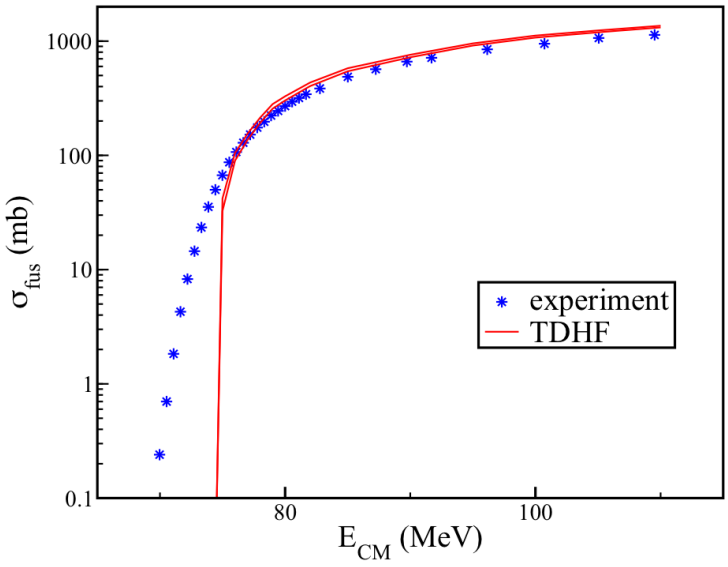

Figure 2.2: Collision energy dependence of fusion cross sections in ^{16}O+^{208}Pb collisions. The blue dots represent experimental results referenced from [26], and the red curve represents the results of TDHF calculations. The two red curves represent the lower and upper limits of the theoretical results, respectively. This figure was taken from [37]

system, where the blue points show the experimental results and the red curve shows the TDHF results. The blue points show the experimental results, and the red curve shows the TDHF results. The comparison of the blue points to the red curves shows that the trend of the experimental results is reproduced, although not exactly, at high energies, while at low energies, the fusion cross section calculated by TDHF is drops to zero below a certain energy. In fact, the energy at which the fusion cross section becomes zero in TDHF coincides with the height of the Coulomb barrier. Since fusion at energies below the Coulomb barrier is always accompanied by quantum tunneling, TDHF yields zero fusion cross section in that region as quantum tunneling cannot be described in TDHF. For this reason, TDHF is mainly used only for reactions above the barrier, and the microscopic description of nuclear reactions in the low energy region has remained a theoretical challenge.

2.2 Beyond Mean-Field theories

Several methods have been developed to go beyond TDHF and resolve the drawbacks of TDHF: underestimation of quantum fluctuations and a failure to describe quantum tunneling phenomena. Here we discuss two examples. In the course of presenting those examples, we will explain how previous methods have solved the drawbacks of TDHF and what has still been unsolved.

2.2.1 Time-Dependent Hill-Wheeler theory

We first discuss the Time-Dependent Hill-Wheeler (TDHW) theory. This theory can describe collective tunneling and is applied to spontaneous fission [19, 20, 70]. One of the concepts of this method is to recover the quantum fluctuations lost in the Hartree-Fock method by superposing static Slater determinants, as shown in the following equation.

$$|\Psi(t)\rangle = \int dq f(q,t) \, |\Phi(q)\rangle \tag{2.19}$$

Here $|\Phi(q)\rangle$ means a Slater determinant state, and q is called the generator coordinate, which is often chosen to be a collective degree of freedom such as the deformation or the center-of-mass motion of the nucleus. This method also describes the dynamics of the wave function by making the weight function of the superposition dependent on time.

For example, if q is the deformation of a nucleus, then Eq. (2.19) is a superposition of Slater determinants that represent the nucleus deformed in different ways. A schematic picture of how TDHW describes the dynamics of a nucleus is shown in Fig. 2.3. As shown in Fig. 2.3, in TDHW, the Slater determinant Φ with different q serves as a basis in q-coordinates, and the weights on a Slater determinant can be viewed as wave functions moving in the q-coordinate space. Strictly speaking, rather than the weight f itself the collective wave function g,

$$g = \mathcal{N}^{\frac{1}{2}} f, \tag{2.20}$$

has to be viewed as a wave function moving in q-coordinate space. Here, $\mathcal{N} = \langle \Phi(q) | \Phi(q') \rangle$ is called norm kernel.

Advantages of TDHW

The reason why this method can recover quantum fluctuations in q-coordinate lost in TDHF and describe quantum tunneling phenomena is as follows. The

Slater determinants on the q-coordinate axis of Fig. 2.3 are each calculated with a static HF, and they are trapped and localized to a self-consistent one-body potential as mentioned in the previous section. However, there is no reason for the weights g on multiple Slater determinants to be localized as in HF, and they are transferred between Slater determinants according to the time-dependent variational principle. In this way, g, which can be regarded as a wave function, is spread wider than the one-body potential of HF, and the quantum fluctuation in q-coordinate is recovered. It is also possible to describe quantum tunneling phenomena in q-coordinate in the same way. Because the TDHF was trapped in a one-body potential, the wave function could not be split and the probabilistic tunneling probability could not be described. In TDHW, on the other hand, the weight g is partially transferred to the Slater determinant prepared behind the barrier (Case (c) in Fig. 2.3), which allows us to describe the probabilistic tunneling probability and thus the quantum tunneling phenomenon.

Drawbacks of TDHW

As described above, TDHW can describe quantum fluctuation and quantum tunneling in q-coordinate space, which is the collective coordinate selected as the generator coordinate. On the other hand, similar to macroscopic approaches, it has a drawback to arbitrarily choose the collective coordinate. In other words, in TDHW, one has to choose a collective coordinate to recover quantum fluctuations according to the system of interest, and the choice is not always obvious. In addition, since Slater determinants prepared in TDHW are usually the ground state prepared in static HF, the effect of internal excitations in the degrees of freedom other than the chosen q-coordinate is ignored in that case. Although it is possible in principle to include Slater determinants with particle-hole excitations as the basis states in TDHW method [71], it is still difficult to determine a priori the appropriate bases for a collision process where non-trivial and complicated excitations may take place. because it is not obvious what kind of excited states should be prepared and also the computational cost increases with the number of prepared states.

2.2.2 Simplified Time-Dependent Generator Coordinate Method

Next, we discuss the simplified Time-Dependent Generator Coordinate Method (simplified TDGCM) introduced by P.-G. Reinhard, R. Y. Cusson, and K. Goeke in 1983 [21]. In this method, time-dependent Slater determinants,

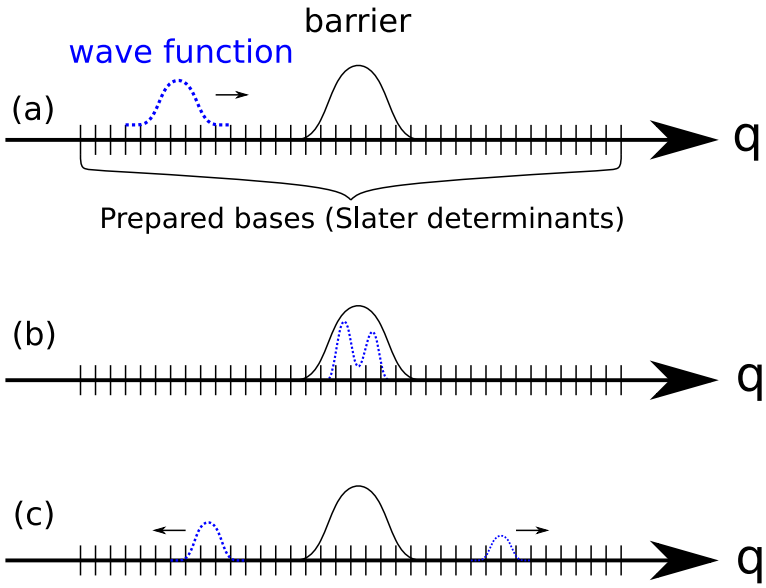

Figure 2.3: Schematic picture of the wave function in TDHW. Time is progressing in the order of (a), (b), and (c). From left to right, the wave function collides with the barrier and probabilistically penetrates the barrier. The short vertical lines placed at the q-coordinates refer to the initially prepared Slater determinant with different q. What we call the wave function here is the weight g defined in Eq. (2.20), which can be understood as the wave function in the space (q-coordinate space) created by the prepared Slater determinant.

evolved independently in time with several initial conditions, are superposed as a trial function of the time-dependent variational method. Since such Slater determinants are nothing more than TDHF states, the wave function is given by

$$|\Psi(t)\rangle = \sum_q f_q(t)\,|\Phi^q_{\rm TDHF}(t)\rangle\,, \tag{2.21}$$

A schematic representation of this method is shown in Fig. 2.4. Basically, the dynamics of a nucleus is expressed by moving the time-varying weight f between the prepared Slater determinants as in TDHW. In this way, quantum fluctuations can be recovered for the same reason as in TDHW. The difference from TDHW is that the Slater determinants evolve in time.

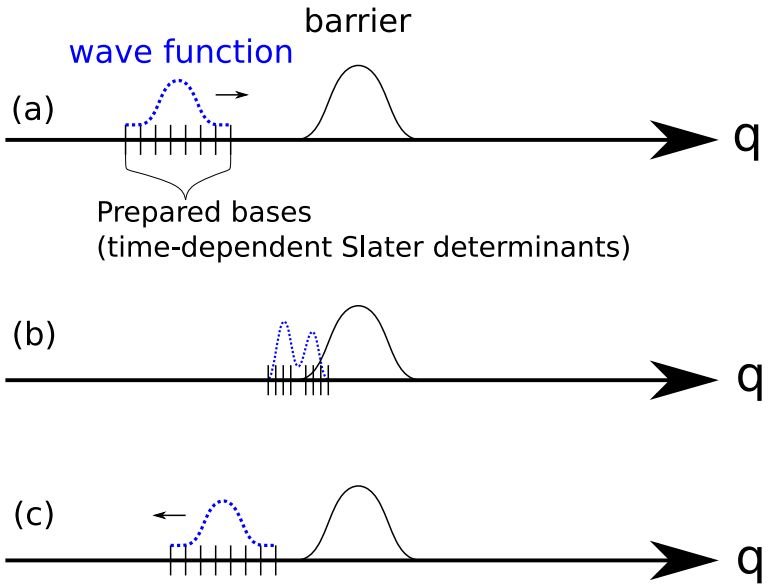

Figure 2.4: Schematic picture of the wave function in simplified TDGCM. Each of the initially prepared Slater determinants evolve in time with TDHF, and the weights on each also evolve in time. If all the Slater determinants have energies less than the barrier, as in the setup of this figure, the Slater determinants will not transmit through the barrier and there will be no component of the wave function to tunnel through.

Advantages of simplified TDGCM

An advantage of using the time-evolving Slater determinants is that the effect of internal excitations of nuclei, which is ignored in TDHW, can be incorporated in simplified TDGCM. In other words, this method can recover the quantum fluctuation while incorporating the effect of internal excitations. It is true that the simplified TDGCM also has an arbitrariness in how the initial state of the Slater determinant is chosen, but those Slater determinants are time-evolved by TDHF and have a distribution of $q(t)$ different from that of q in the initial state. Furthermore, the collective coordinate that is not chosen as the generator coordinate also changes according to TDHF. As a result, it is not necessary to prepare all the collective coordinates of interest as in TDHW, but the degrees of freedom necessary to describe the phenomenon are automatically incorporated by the TDHF Slater determinants.

Drawbacks of simplified TDGCM

On the other hand, quantum tunneling cannot be easily described by this method. The reason for this is that Slater determinants for the energies below the barrier cannot be placed beyond the barrier using the usual simplified TDGCM calculation method. In TDHW, static Slater determinants are placed before, after, and inside the barriers to enable the weight transfer between them and to describe the tunneling effect. On the other hand, the basic policy of the simplified TDGCM is to prepare Slater determinants only in front of the barrier as shown in Fig. 2.4, and to move each Slater determinant along with the progress of the nucleus. However, since each Slater determinant is evolving in time by TDHF, those with energies lower than the barrier will never cross the barrier, and as a result, there can be no Slater determinant with energies lower than the barrier on the other side of the barrier. As an extreme example, if one prepare only Slater determinants with energies lower than the barrier as the initial state, no small component of the wave function will ever cross the barrier.

Another drawback to mention is that the time-evolved Slater determinant in TDHF is not necessarily the best way to represent the system. When considering the superposition of Slater determinants, there should be an optimal cooperative behavior of the individual Slater determinants. However, in the simplified TDGCM, each Slater determinant evolves in time by TDHF independently, so such cooperation is not possible.

2.2.3 Remaining problems

In this section, we have introduced two methods that partially solve the drawbacks of TDHF. TDHW enables a description of quantum fluctuations and quantum tunneling, but this method has the disadvantage of arbitrarily restricting the collective degrees of freedom and consequently neglects the various internal excitations of nuclei. On the other hand, the simplified TDGCM can recover the quantum fluctuation while incorporating the effect of internal excitations of nuclei, but it is hard to describe the quantum tunneling phenomenon with this method. Other methods beyond TDHF have been devised, but no theory has yet been developed that can describe the tunneling effect while automatically incorporating the effect of internal excitations through microscopic calculations. Such a theory is essential for fusion reactions at energies below the Coulomb barrier, because various internal excitations play an important role in the fusion reaction, and fusion below the Coulomb barrier occurs only with quantum tunneling. In the following chapters, we will present a method that can resolve this problem.

Chapter 3

Time-Dependent Generator Coordinate Method

As explained in the previous chapter, the mean-field approximation considerably underestimates the quantum fluctuation and fails to describe quantum tunneling. In order to overcome such drawbacks, several beyond-mean-field method have been considered, for example the time-dependent Hill-Wheeler equation for fission dynamics with tunneling and the stochastic mean-field theory for restoring the quantum fluctuation as mentioned in Sec. 2.2. However, there is still no microscopic theory for low-energy fusion reactions which is required to include the nonadiabatic internal excitation and describe the quantum tunneling effect. That is why we aim to develop the Time-Dependent Generator Coordinate Method (TDGCM) [22], which have such ability to describe low-energy fusion reactions. Since TDGCM is based on the time-dependent variational principle, we start with its explanation.

3.1 Time-Dependent Variational Principle (TDVP)

The time-dependent variational principle is one of the approximate ways to solve the Schrödinger equation. Here, we introduce the general concept of the time-dependent variational principle [83]. In quantum mechanics, the time evolution of a state is given by the time-dependent Schrödinger equation

$$i\hbar\frac{\partial}{\partial t}\left|\Psi(t)\right\rangle = \hat{H}\left|\Psi(t)\right\rangle, \tag{3.1}$$

where $\hat{H}$ is the Hamiltonian and $|\Psi(t)\rangle$ is the state. This equation can be derived from the variation of the action [84–89]

$$A' = \int_{t_1}^{t_2} dt \mathcal{L}'(\Psi(t)^*, \Psi(t), \dot{\Psi}(t)), \tag{3.2}$$

where the Lagrangian $\mathcal{L}'$ is written as

$$\mathcal{L}'(\Psi(t)^*, \Psi(t), \dot{\Psi}(t)) = \left\langle \Psi(t) \left| i\hbar \frac{\partial}{\partial t} - \hat{H} \right| \Psi(t) \right\rangle. \tag{3.3}$$

The Ψ and Ψ^* may be regarded as independent variables. By using Eq. (3.3), under the condition that the action takes an local minimum, the variation of the action with respect to Ψ^* is written as

$$\delta A' = \int_{t_1}^{t_2} dt \left\langle \delta\Psi(t) \left| i\hbar \frac{\partial}{\partial t} - \hat{H} \right| \Psi(t) \right\rangle. \tag{3.4}$$

where the variation at the end points are fixed $\delta\Psi(t_1) = \delta\Psi(t_1)^* = \delta\Psi(t_2) = \delta\Psi(t_2)^* = 0$. If $|\Psi\rangle$ is not restricted in Hilbert space, the variation $\langle\delta\Psi(t)|$ can be taken arbitrarily. Therefore, we obtain

$$\left(i\hbar \frac{\partial}{\partial t} - \hat{H} \right) |\Psi(t)\rangle = 0, \tag{3.5}$$

which is nothing but the Schrödinger equation Eq. (3.1). For this property, it is expected that a reasonable restriction in Ψ will lead to a good approximation of the full problem.

3.1.1 For restricted state

Let us consider a state $|Q'(t)\rangle$ which is parametrized by a set of complex variables $Q'(t) = \{q_0(t), q_1(t), q_2(t), ...\}$. We assume that the q_0 is overall factor in the sense

$$|Q'(t)\rangle = q_0(t) |Q(t)\rangle = q_0(t) |q_1(t), q_2(t), ...\rangle, \tag{3.6}$$

and $|Q(t)\rangle$ depends on time implicit only through the variables $q(t)$. It is also assumed that $|Q\rangle$ is given as a function of q only and does not explicitly depend on q^*.

Variation of the action (3.2) with the Lagrangian (3.3) with respect to $Q'^*(t)$ leads to

$$\delta A' = \int_{t_1}^{t_2} dt \sum_{\nu} \delta q_\nu^*(t) \left(\frac{\partial}{\partial q_\nu^*} \langle Q'(t)| \right) \left(i\hbar \frac{\partial}{\partial t} - \hat{H} \right) |Q'(t)\rangle = 0. \tag{3.7}$$

Since $\delta q_\nu^*(t)$ can be chosen arbitrarily, the following equation are fulfilled for extremal action:

$$\left(\frac{\partial}{\partial q_\nu^*}\langle Q'(t)|\right)\left(i\hbar\frac{\partial}{\partial t}-\hat{H}\right)|Q'(t)\rangle = 0. \tag{3.8}$$

Eq. (3.8) can be rewritten as

$$i\hbar\sum_\nu C'_{\mu\nu}\dot{q}_\nu = \frac{\partial}{\partial q_\mu^*}\langle Q'(t)|\hat{H}|Q'(t)\rangle\,, \tag{3.9}$$

where

$$C'_{\mu\nu} = \frac{\partial^2}{\partial q_\mu^*\partial q_\nu}\langle Q'(t)|Q'(t)\rangle\,. \tag{3.10}$$

In the case of the restricted variation, the equations of motion for the variational parameters are derived from variation. Eqs. (3.9) and (3.10) define the time evolution of the state $|Q'(t)\rangle$.

For the sake of simplicity, we express the overall factor q_0 in terms of the other variables. To this end, we rewrite the Euler-Lagrange equations

$$\begin{aligned}\frac{d}{dt}\frac{\partial\mathcal{L}'}{\partial\dot{q}_\nu^*}-\frac{\partial\mathcal{L}'}{\partial q_\nu^*} &= 0\\ &= \left(\frac{d}{dt}\frac{\partial\mathcal{L}}{\partial\dot{q}_\nu^*}-\frac{\partial\mathcal{L}}{\partial q_\nu^*}\right)q_0q_0^*\langle Q|Q\rangle\\ &\quad+\frac{d}{dt}(|q_0|^2\langle Q|Q\rangle)\frac{\partial\mathcal{L}}{\partial\dot{q}_\nu^*}+|q_0|^2(i\dot{q}+\mathcal{L})\frac{\partial\langle Q|Q\rangle}{\partial q_\nu^*},\end{aligned} \tag{3.11}$$

where a new Lagrangian $\mathcal{L}$ is defined by

$$\mathcal{L}(Q^*,Q,\dot{Q}^*,\dot{Q}) = \frac{i}{2}\left(\frac{\langle Q|\dot{Q}\rangle-\langle\dot{Q}|Q\rangle}{\langle Q|Q\rangle}\right)-\frac{\langle Q|H|Q\rangle}{\langle Q|Q\rangle} \tag{3.12}$$

$$\equiv \mathcal{L}_0(Q^*,Q,\dot{Q}^*,\dot{Q})-\mathcal{H}(Q^*,Q). \tag{3.13}$$

By using two conditions from normalization of state $|Q'\rangle$ and Eq. (3.8)

$$\begin{cases}|q_0|^2 &= \frac{1}{\langle Q|Q\rangle}\\ \dot{q}_0 &= i\mathcal{L},\end{cases} \tag{3.14}$$

the last two terms in Eq. (3.11) vanish. Then we obtain the Euler-Lagrange equation for a new Lagrangian $\mathcal{L}$

$$\frac{d}{dt}\frac{\partial\mathcal{L}}{\partial\dot{q}_\nu^*}-\frac{\partial\mathcal{L}}{\partial q_\nu^*} = 0, \tag{3.15}$$

where the overall term q_0 no longer exists. The Euler-Lagrange equation can be transformed to obtain the Hamilton's equation:

$$i\hbar \sum_{\nu} \mathcal{C}_{\mu\nu} \dot{q}_{\nu} = \frac{\partial \mathcal{H}}{\partial q_{\mu}^{*}}, \tag{3.16}$$

where the Hermitian matrix $\mathcal{C}$ is given by

$$\mathcal{C}_{\mu\nu} = \frac{\frac{\partial}{\partial q_{\mu}^{*}} \frac{\partial}{\partial q_{\nu}} \langle Q|Q\rangle}{\langle Q|Q\rangle} - \frac{\frac{\partial}{\partial q_{\mu}^{*}} \langle Q|Q\rangle}{\langle Q|Q\rangle} \frac{\frac{\partial}{\partial q_{\nu}} \langle Q|Q\rangle}{\langle Q|Q\rangle} \tag{3.17}$$

$$= \frac{\partial}{\partial q_{\mu}^{*}} \frac{\partial}{\partial q_{\nu}} \ln \langle Q|Q\rangle \,. \tag{3.18}$$

We will next explain TDGCM using TDVP.

3.2 Overview of Time-Dependent Generator Coordinate Method (TDGCM)

The TDGCM is based on the time-dependent variational method with the trial wave function

$$|\Psi(t)\rangle = \int da f_a(t) \, |\Phi_a(t)\rangle \,, \tag{3.19}$$

where $|\Phi_a(t)\rangle$ is a Slater determinant and $f_a(t)$ is a weight function. Note that the Slater determinants are non-orthogonal to each other. The index a is called a generator coordinate, and usually the collective coordinates are used for this. The feature of this method is a superposition of time-dependent Slater determinants $|\Phi_a(t)\rangle$. The superposed Slater determinant mimic the time-evolution of the quantum mechanical wave function in the selected collective coordinate. In the demonstration of TDGCM in Chap. 4, We have chosen the center-of-mass position and center-of-mass momentum as the generator coordinates, and then the TDGCM wave functions mimic the quantum mechanical wave function of the center-of-mass position and momentum plane.

3.2.1 Comparison with existing theories

In this section, we will compare TDGCM with the two methods listed in Sec. 2.2. The difference between TDHW and TDGCM is whether or not internal excitations are taken into account. In TDHW, the Slater determinants used for superposition are static, as shown in the equation, and they

are usually in the ground state. Because of this superposition of static Slater determinants, TDHW usually ignores internal excitations and is not suitable for fusion where internal excitations play an important role. There is also an attempt to incorporate the effects of excited states in TDHW [71], but this method also requires pre-selection of the excited states to be included, and is difficult to use in a fusion where it is not obvious what excitations will be important. On the other hand, the trial function used in TDGCM is a superposition of time-dependent Slater determinants, and hence can consider internal excitations as well as TDHF.

Next, we compare our TDGCM with simplified TDGCM. The difference between TDGCM and simplified TDGCM is the ability to describe the tunneling effect. Simplified TDGCM was introduced to recover quantum fluctuations in the dynamics of nuclei, and has never been applied to describe the tunneling effect. However, the trial function used in simplified TDGCM uses time-dependent Slater determinants calculated with independent TDHFs, which do not overcome the barrier if they originally have an energy smaller than the barrier. Considering an extreme case, if the initially prepared wave packet does not contain any component with energy exceeding the barrier, i.e., no Slater determinant with energy greater than the barrier, the barrier transmission probability will be zero in simplified TDGCM. However, in quantum mechanics, even if the initial wave function does not contain a component with energy larger than the barrier, the tunneling effect can still result in a finite barrier transmission probability. In contrast, in our TDGCM, the superimposed Slater determinants evolve in time in relation to each other, and a finite barrier transmission probability is obtained even in the extreme case described above. Specifically, the superimposed Slater determinants exchange energy with each other through overlap between them, and some Slater determinants are able to cross the barrier even if initial energy is lower than the barrier.

3.3 TDGCM with Gaussian single-particle wave functions

TDGCM has not only the advantages but also a disadvantage, that is a huge calculation cost. Naively there are many degrees of freedom, multi Slater determinants and their weights. Note that only a single Slater determinant is used in TDHF. In order to reduce the calculation cost, we introduce in this thesis the Gaussian form of single-particle wave functions based on the idea of Antisymmetrized Molecular Dynamics (AMD) [74, 75]. First of all,

we will give a brief explanation of AMD.

3.3.1 Antisymmetrized Molecular Dynamics

AMD is an approximation method that restricts the single-particle wave function of the Slater determinant used in TDHF to the form of a Gaussian function. In other words, it is an additional approximation to TDHF. In many papers, the collision term, which represents direct nucleon collisions, is introduced in AMD, but we will not use it in this thesis. In AMD, we use a single-particle wave function of the following form

$$\phi_i(\vec{x}) = e^{-\nu\left(\vec{x}-\frac{z_i}{\sqrt{\nu}}\right)^2}\chi_{\sigma_i}\chi_{\tau_i}, \tag{3.20}$$

where the subscript i is the index of the single-particle state, and χ_{σ_i} and χ_{τ_i} are the spin and isospin wave function respectively. Here, ν is the Gaussian width and z_i is the Gaussian center. While ν is usually real, z_i is complex, and the real and imaginary parts of z are related to the expectation value of potision $\bar{x}$ and momentum $\bar{k}$ of the single-particle wave function as follows,

$$\bar{x} = \frac{\mathrm{Re}(z)}{\sqrt{\nu}} \tag{3.21}$$

$$\bar{k} = 2\sqrt{\nu}\mathrm{Im}(z). \tag{3.22}$$

Another way to describe it is as follows

$$z(t) = \sqrt{\nu}\bar{x} - i\frac{\bar{k}}{2\sqrt{\nu}}. \tag{3.23}$$

In other words, the dynamics of the single-particle wave function is determined by z. Using this single-particle wave function, the Slater determinant becomes

$$\Phi(\vec{x}_1, \vec{x}_2, ..., t) = \mathcal{A}(\phi_i(\vec{x}_1, t)\phi_j(\vec{x}_2, t)\cdots\phi_n(\vec{x}_A, t)\chi_{\sigma_i}\chi_{\tau_i}\chi_{\sigma_j}\chi_{\tau_j}\cdots\chi_{\sigma_n}\chi_{\tau_n}) \tag{3.24}$$

$$= \mathcal{A}\left(e^{-\nu\left(\vec{x}_1-\frac{z_i(t)}{\sqrt{\nu}}\right)^2}e^{-\nu\left(\vec{x}_2-\frac{z_j(t)}{\sqrt{\nu}}\right)^2}\cdots e^{-\nu\left(\vec{x}_A-\frac{z_n(t)}{\sqrt{\nu}}\right)^2}\chi_{\sigma_i}\chi_{\tau_i}\chi_{\sigma_j}\chi_{\tau_j}\cdots\chi_{\sigma_n}\chi_{\tau_n}\right), \tag{3.25}$$

where $\mathcal{A}$ is antisymmetrizer. By using this wave function as a trial function and applying the time-dependent variational principle, the equation of motion for the single-particle wave function in AMD can be obtained.

One thing that is characteristic of the AMD wave function is that the wave function can be analytically divided into a center-of-mass part and an intrinsic part,

$$\begin{aligned}\Phi &= \mathcal{A}\left(e^{-\nu(r_1-\frac{z_i}{\sqrt{\nu}})^2}\cdots\chi_{\sigma_i}\chi_{\tau_i}\right)\\ &= e^{-A\nu(R_G-z_G/\sqrt{\nu})^2}\mathcal{A}\left(e^{-\nu(r_1-R_G-\frac{z_i-z_G}{\sqrt{\nu}})^2}\cdots\chi_{\sigma_i}\chi_{\tau_i}\right) \qquad (3.26)\\ &= \Phi_G\times\Phi_{\rm int}, \qquad (3.27)\end{aligned}$$

where $R_G=\frac{\sum_i x_i}{A}$ and $z_G=\frac{\sum_i z_i}{A}$. Here, Φ_G and $\Phi_{\rm int}$ are the conter-of-mass and intrinsic part of the wave function, respectively. Note that, as can be seen from the Eq. (3.26), the center-of-mass wave function in AMD has the form of a Gaussian function, and the width is determined by the Gaussian width of the single-particle wave function, ν.

3.3.2 TDGCM with AMD single-particle wave functions

Bringing the Gaussian single-particle wave functions introduced in the previous subsection into TDGCM, we obtain the following TDGCM wave function Ψ the spatial part of the trial wave function $\Psi(\vec{x},t)$ is

$$\begin{aligned}\Psi(\vec{x}_1,\vec{x}_2,...,t) &= \sum_a f_a(t)\Phi_a(\vec{x}_1,\vec{x}_2,...,t) \qquad (3.28)\\ &= \sum_a f_a(t)\mathcal{A}(\phi_{ia}(\vec{x}_1,t)\phi_{ja}(\vec{x}_2,t)\cdots\phi_{na}(\vec{x}_A,t)) \qquad (3.29)\\ &= \sum_a f_a(t)\mathcal{A}\left(e^{-\nu\left(\vec{x}_1-\frac{z_{ia}(t)}{\sqrt{\nu}}\right)^2}e^{-\nu\left(\vec{x}_2-\frac{z_{ja}(t)}{\sqrt{\nu}}\right)^2}\cdots e^{-\nu\left(\vec{x}_A-\frac{z_{na}(t)}{\sqrt{\nu}}\right)^2}\right). \qquad (3.30)\end{aligned}$$

where $\mathcal{A}$ is the antisymmetrizer, and ϕ_{ia} is single-particle wave function.

In addition, in this thesis, we assume that the Gaussian width of each single-particle wave function is common and fixed. Under this assumption, by using Gaussian single-particle wave function, the number of degrees of freedom of the trial function becomes

$$N_a + N_a\times A\times D, \qquad (3.31)$$

where N_a is the number of superposed Slater determinants: the N_a in the first term means the number of weight functions, and the N_a in the second term

means the number of Slater determinants. A is the number of nucleons and D is the number of dimensions we are considering. If we use an unrestricted single-particle wave function and solve in a grid-delimited space, the number of degrees of freedom in the trial function is

$$N_a + N_a \times A \times N_{\text{grid}}^D, \tag{3.32}$$

where N_{grid} is the number of grid points on a single coordinate axis. In fusion calculations, N_{grid} is usually in the order of a hundred to a thousand, and the Gaussian single-particle wave function can reduce the number of degrees of freedom remarkably, especially in 3D calculations.

3.3.3 Interpretation of TDGCM wave function

Since TDGCM is a method based on the time-dependent variational principle, its solution is expected to mimic the solution of the time-dependent Schrodinger equation. Therefore, in order to understand how the wave function of TDGCM evolves in time, we compare it with the time evolution of the wave function in quantum mechanics and AMD. To simplify the discussion, we will consider only the center-of-mass wave function and ignore the internal excitations. It should be noted that the wave function treated in TDGCM and TDHF is a wave packet, and unlike a plane wave, it contains several different momentum components. In the following, we consider a wave packet centered at a positive x as the initial state in one-dimensional space, and consider the time evolution when the entire wavepacket is boosted in the $-x$ direction, that is, e^{ikx} is multiplied by the wavepacket with a negative momentum k. In this case, there is no external barrier and the wave packet is in free motion. Starting from the above initial conditions, the time evolution is illustrated in phase space in Fig. 3.1, Fig. 3.2, and Fig. 3.3, for quantum mechanics, AMD, and TDGCM, respectively. The left side of each figure shows the initial state, and the right side shows the state after a certain time. The solid circle represents the contour line of the Wigner function defined as

$$P(x,k) = \frac{1}{\pi\hbar}\int_{-\infty}^{\infty} \psi^*(x+y)\psi(x-y)e^{2ipy/\hbar}dy. \tag{3.33}$$

The Wigner function is like a probability density distribution on phase space. The center-of-mass position of the Slater determinant in phase space is indicated by a cross mark in TDGCM and AMD. Multiple cross marks exist in TDGCM because multiple Slater determinants are used.

First, let us look at the time evolution of quantum mechanics shown in Fig. 3.1. A characteristic feature of the free motion of wave packets in

quantum mechanics is that they expand spatially with time. This is due to the fact that the wave packet contains components with different momenta, and it can be understood that the component of the wave packet with higher momenta precedes further than the component with lower momenta. Note here that the wave packet does not spread in momentum space. On the other hand, in the time evolution of the wave packet in AMD, the wave packet spreads in neither coordinate space nor momentum space, due to the condition we applied to fix the Gaussian width of the single-particle wave function. In contrast, in TDGCM, the trial function is a superposition of Slater determinants. By using such trial functions, the spread of the wave packet is restored. Although each superimposed Slater determinant is a wavepacket with no broadening, as in the AMD case, the broadening of the TDGCM wavefunction as a whole is expressed by changing the distance between the Slater determinants.

Next, let us look at how the wave packet transmits over the barrier. In Fig. 3.1, Fig. 3.2, and Fig. 3.3, there is a dotted line at the momentum corresponding to the height of the barrier. This means that the component of the wave packet below the dotted line already has a larger energy than the barrier in the initial state. First of all, in the case of quantum mechanics shown in Fig. 3.1, the component of wave packet that already has energy above the barrier in its initial state will classically pass through the barrier. In addition, even components with energy lower than the barrier will probabilistically pass through the barrier, which is called the quantum tunneling effect. In this way, when a wave packet in quantum mechanics collides with a barrier, it can be divided into two components: one that is transmitted through the barrier and the other that is reflected by the barrier. It is important to note that, since we are now considering the center-of-mass part of the many-body wave function, the division of the wave packet does not mean that only some particles will penetrate the barrier, but that all particles will probabilistically be transmitted or reflected at the same time. In contrast, the wave packet in AMD is classical in a sense. In other words, AMD allows only a discrete transmission probability of 0 or 1, meaning that if the expected momentum of the wave packet exceeds the barrier, the entire wave packet will be transmitted through the barrier,and if not, the entire wave packet will be reflected by the barrier. Because of this feature, AMD cannot express the quantum tunneling effect, nor the continuous barrier transmission probability as a function of energy. On the other hand, TDGCM can describe quantum tunneling phenomena and continuous tunneling probabilities by superposition of time-dependent Slater determinants with time-dependent weights. First of all, since the wave packet in the TDGCM is made of a superposition of Slater determinants, it is possible for a component with an energy already

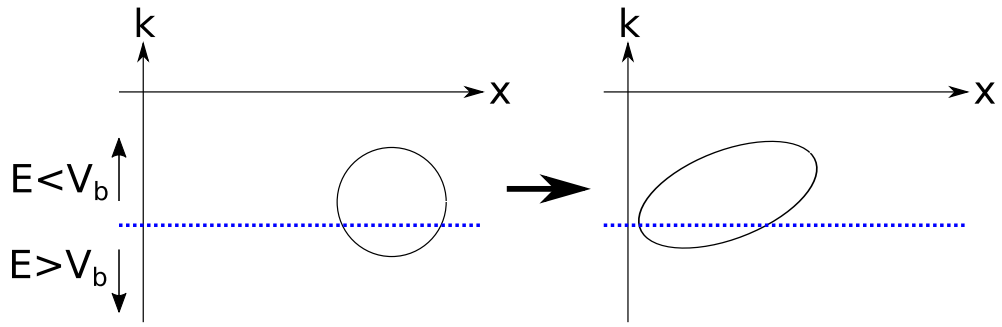

Figure 3.1: The time evolution of the wave packet in quantum mechanics. In the quantum mechanics, the initial wave packet change its shape because the wave packet is superposition of several momentum eigenstates which have different eigenvalue. The component which have larger absolute value of momentum go ahead before the component which have smaller absolute value of momentum. Consequently the spatial width of wave packet become wider. In contrast, the width in momentum space does not change. In the case that the potnetial barrier exists, the component in the region that the energy E is larger than the barrier height V_b overcome the barrier and is split from the rest wave packet which is reflected by the potential barrier. Even if the energy of component is less than the barrier height, some part of component penetrate the potential barrier due to the qunatum tunneling effect.

greater than the barrier to partially penetrate in the initial condition, just like the wave packet in quantum mechanics. In addition, the quantum tunneling effect is expressed when some of Slater determinants cross the barrier by exchanging energy among the Slater determinants, even though the initial condition has less energy than the barrier. Furthermore, since the weight function of the TDGCM is also determined by the time-dependent variational principle, weights are assigned to the Slater determinant transmitted through the barrier and the Slater determinant reflected by the barrier, mimicking quantum mechanics, resulting in a continuous barrier transmission probability as a function of energy, similar to that obtained in quantum mechanics.

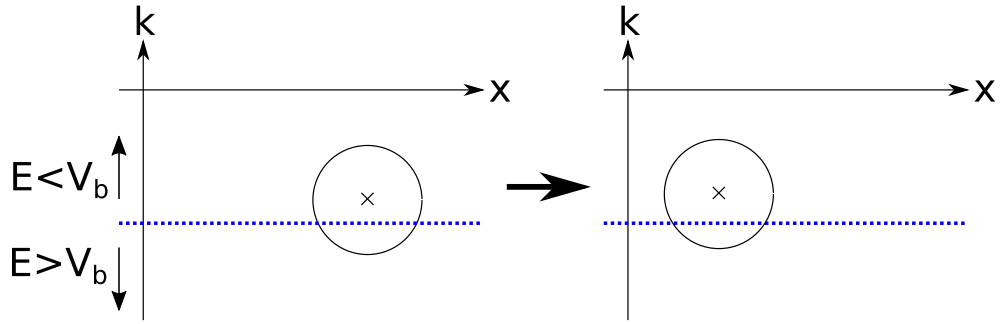

Figure 3.2: The time evolution of the wave packet in AMD. In the case that the Gaussian width is fixed as in our calculation, the wave packet does not change its shape. In contrast to the quantum mechanics, AMD wave packet does not split to the component which overcome the barrier and the rest which reflected by the barrier. The whole wave packet overcome the barreir if the energy expectation of the AMD wave packet is larger than the barreir and reflected by the barrier if not, that is, the transmission probability is always 0 or 1 in AMD framework.

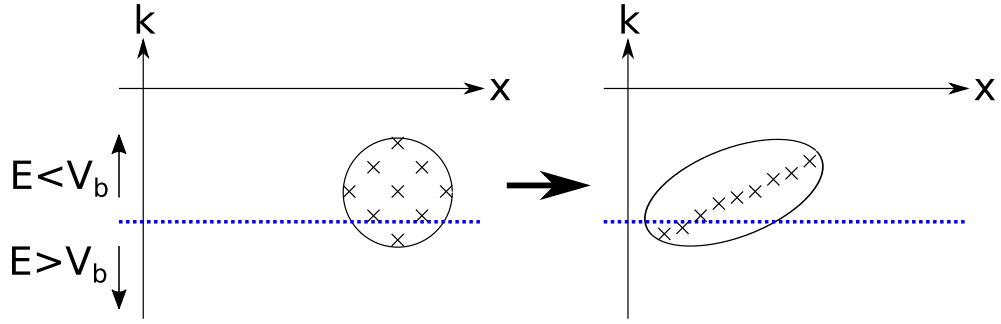

Figure 3.3: The time evolution of the wave packet in TDGCM. The wave packet in TDGCM framework is represented by the multi Gaussian wave packets and the weights for each Gaussian under the restrictions as in our calculation. The time evolution of each Gaussian wave packet and their weights are determined by the time-dependent variational principle in order to mimic the time evolution of the wave packet in the quantum mechanics. The split of the wave packet as in the quantum mechanics can be represented by the multi Gaussian wave packets, that is, the multi Gaussian wave packets split into ones which transmit the barrier and the rest which reflected by the barrier.

Chapter 4

Application of time-dependent generator coordinate method

In this chapter, we apply TDGCM to three simple systems with ^{4}He particles. First, we apply the TDGCM to a one-dimensional ^{4}He+^{4}He collision system and qualitatively demonstrate that the TDGCM is a framework that can describe quantum tunneling phenomena. At the same time, we discuss the mechanism by which TDGCM can describe quantum tunneling phenomena. However, there is a problem in examining in detail the barrier transimission probability that can be calculated by TDGCM in this ^{4}He+^{4}He system, so we next applied TDGCM to a system where ^{4}He collides with an external barrier in one dimension. The application to this system shows that the TDGCM can calculate the smooth transmission probability as a function of collision energy. Finally, we perform the TDGCM calculations in three dimensions, which is necessary to apply the TDGCM to realistic calculations. We show that the TDGCM can describe quantum tunneling in ^{4}He+^{4}He collisions in three dimensions as well as in one dimension.

In the following calculations, we make an assumption that the Gaussian center for all the nucleons in each ^{4}He particles is identical for simplicity of the calculations. This means that we take $z_{p\uparrow} = z_{p\downarrow} = z_{n\uparrow} = z_{n\downarrow} \equiv z$ for nucleons in each ^{4}He, where the subscript p means proton, n means neutron, and the up and down arrows mean spin up and down, respectively. This means that there is no transfer of nucleons between nuclei.

4.1 Equations of motion for TDGCM with Gaussian single-particle wave function

We will first explain the equation of motion of the wave function of the TDGCM under the above assumption. Since the variational parameters in the wave function Eq. (3.30) are f_a and z_a, the variational equations Eq. (3.16) are written as

$$i\hbar \sum_\nu C_{\mu\nu}\dot{z}_\nu = \frac{\partial \mathcal{H}}{\partial z^*_\mu}, \tag{4.1}$$

$$i\hbar \sum_\nu C_{\mu\nu}\dot{f}_\nu = \frac{\partial \mathcal{H}}{\partial f^*_\mu}, \tag{4.2}$$

which give the time evolution of the Gaussian center z_a and the weight f_a. Using the explicit form of the wave function Eq. (3.30), $C_{\mu\nu}$ is written by z_a and f_a as following three combinations

$$C_{\mu\nu} \to \begin{cases} C_{f_\mu f_\nu} = & \frac{\partial_{f^*_\mu}\partial_{f_\nu}\langle\Psi|\Psi\rangle}{\langle\Psi|\Psi\rangle} - \frac{\partial_{f^*_\mu}\langle\Psi|\Psi\rangle}{\langle\Psi|\Psi\rangle}\frac{\partial_{f_\nu}\langle\Psi|\Psi\rangle}{\langle\Psi|\Psi\rangle} \\ C_{f_\mu z^\nu_k} = & \frac{\partial_{f^*_\mu}\partial_{z^\nu_k}\langle\Psi|\Psi\rangle}{\langle\Psi|\Psi\rangle} - \frac{\partial_{f^*_\mu}\langle\Psi|\Psi\rangle}{\langle\Psi|\Psi\rangle}\frac{\partial_{z^\nu_k}\langle\Psi|\Psi\rangle}{\langle\Psi|\Psi\rangle} \\ C_{z^\mu_i z^\nu_j} = & \frac{\partial_{z^{\mu*}_i}\partial_{z^\nu_j}\langle\Psi|\Psi\rangle}{\langle\Psi|\Psi\rangle} - \frac{\partial_{z^{\mu*}_i}\langle\Psi|\Psi\rangle}{\langle\Psi|\Psi\rangle}\frac{\partial_{z^\nu_j}\langle\Psi|\Psi\rangle}{\langle\Psi|\Psi\rangle} \end{cases}, \tag{4.3}$$

where the first derivatives are given by

$$\partial_{f_\nu}\langle\Psi|\Psi\rangle = \sum_a f^*_a \langle\Phi_a|\Phi_\nu\rangle, \tag{4.4}$$

$$\partial_{z^\nu_k}\langle\Psi|\Psi\rangle = \sum_a f^*_a f_\nu \langle\Phi_a|\Phi_\nu\rangle \sum_j (z^{a*}_j - z^\nu_k) B^{a\nu}_{jk}(B^{a\nu})^{-1}_{kj}, \tag{4.5}$$

and the second derivatives are given by

$$\partial_{f^*_\mu}\partial_{f_\nu}\langle\Psi|\Psi\rangle = \langle\Phi_\mu|\Phi_\nu\rangle, \tag{4.6}$$

$$\partial_{f^*_\mu}\partial_{z^\nu_k}\langle\Psi|\Psi\rangle = f^*_\mu f_\nu \langle\Phi_\mu|\Phi_\nu\rangle \sum_j (z^{\mu*}_j - z^\nu_k) B^{\mu\nu}_{jk}(B^{\mu\nu})^{-1}_{kj} \tag{4.7}$$

$$\begin{aligned} &\partial_{z^{\mu*}_i}\partial_{z^\nu_j}\langle\Psi|\Psi\rangle = f^*_\mu f_\nu \langle\Phi_\mu|\Phi_\nu\rangle \times \\ &((1-(z^{\mu*}_i - z^\nu_j)^2) B^{\mu\nu}_{ij}(B^{\mu\nu})^{-1}_{ji} \\ &- \sum_{kl}(z^{\mu*}_i - z^\nu_k)(z^{\mu*}_l - z^\nu_j) B^{\mu\nu}_{ik}(B^{\mu\nu})^{-1}_{ki} B^{\mu\nu}_{lj}(B^{\mu\nu})^{-1}_{jl} \\ &+ \sum_{kl}(z^{\mu*}_k - z^\nu_j)(z^{\mu*}_i - z^\nu_l) B^{\mu\nu}_{kj}(B^{\mu\nu})^{-1}_{ji} B^{\mu\nu}_{il}(B^{\mu\nu})^{-1}_{lk}). \end{aligned} \tag{4.8}$$

B^{ab} in the above equations are the overlap matrix between single-particle wave functions in Φ_a and Φ_b,

$$\begin{aligned} B^{ab}_{ij} &= \left(B^{ab}\right)_{ij} = \langle \phi^a_i | \phi^b_j \rangle \\ &= \int dx e^{-\nu\left(x-\frac{z^{a*}_i}{\sqrt{\nu}}\right)^2} e^{-\nu\left(x-\frac{z^b_j}{\sqrt{\nu}}\right)^2} \\ &= e^{-\frac{(z^{a*}_i - z^b_j)^2}{2}}. \end{aligned} \tag{4.9}$$

The overlap between Slater determinants are written by B as

$$\langle \Phi_a | \Phi_b \rangle = \det B^{ab}, \tag{4.10}$$

and then the norm of the whole wave function $|\Psi\rangle$ is written as

$$\langle \Psi | \Psi \rangle = \sum_{ab} f^*_a f_b \langle \Phi_a | \Phi_b \rangle = \sum_{ab} f^*_a f_b \det B^{ab}. \tag{4.11}$$

The explicit form of the derivative of the Hamiltonian $\frac{\partial \mathcal{H}}{\partial q^*_\mu}$ will be given in the following sections.

4.2 Application to collision of ^{4}He+^{4}He

In this section, we will discuss whether the TDGCM can penetrate the Coulomb barrier in the collision of two ^{4}He particles.

4.2.1 Setup

For this purpose, we apply TDGCM to the ^{4}He+^{4}He collision in one dimension. In this calculation, we assume that the two ^{4}He move symmetrically with respect to $x = 0$. This assumption means that when one ^{4}He particle has a Gaussian center of $z(t)$, the other ^{4}He particle has a Gaussian center of $-z(t)$. With these approximations, each Slater determinant $\Phi_a(t)$ is parametrized by the only one single variational parameter, $z_a(t)$.

Initially, we construct each Slater determinant $\Phi_z(t = 0)$ which represent the two ^{4}He particles at $x = \pm x_{a0}$, with the momentum of $p = \mp p_{a0}$, respectively. According to the Eq. (3.23), the initial value of the Gaussian center z_a becomes

$$z_a(t = 0) = x_{a0}\sqrt{\nu} - i\frac{p_{a0}}{2\sqrt{\nu}\hbar}. \tag{4.12}$$

We employ the same one dimensional Hamiltonian as the one in [21] with a soft-core Coulomb interaction [76–80] between two protons which is written as

$$v_C(x,x') = \frac{e^2}{\sqrt{\alpha^2+(x-x')^2}}. \tag{4.13}$$

With this Hamiltonian, the matrix element of Hamiltonian is obtained as [81]

$$\begin{aligned}\langle\Phi_a|H|\Phi_b\rangle = \langle\Phi_a|\Phi_a\rangle \int dx \Bigg\{ & \frac{\hbar}{2m}\tau_{ab}(x) + \frac{t_3}{3}\rho_{ab}^3(x) \\ & + \frac{t_0}{2}\rho_{ab}(x)\int dx'\rho_{ab}(x')\frac{b}{\sqrt{\pi}}e^{-\frac{(x-x')^2}{b^2}} \\ & + \frac{e^2}{2}\rho_{ab(p)}(x)\int dx'\rho_{ab(p)}(x')\frac{1}{\sqrt{a^2+(x-x')^2}}\Bigg\},\end{aligned} \tag{4.14}$$

with transition kinetic energy density τ and transition density ρ,

$$\tau_{ab}(x) = \sum_{i,j}\left(\partial_x\phi_{ai}^*\right)\left(\partial_x\phi_{bj}\right)\left(B_{ab}^{-1}\right)_{ji} \tag{4.15}$$

$$\rho_{ab}(x) = \sum_{i,j}\phi_{ai}^*\phi_{bj}\left(B_{ab}^{-1}\right)_{ji}, \tag{4.16}$$

where the single-particle wave function, the matrix B_{ab} and the overlap matrix $\langle\Phi_a|\Phi_b\rangle$ are defined in Eq. (3.20),Eq. (4.9) and Eq. (4.10) respectively. In the Eq. (4.14), the first term in the integral is the kinetic energy term, the second term is the zero-range three-body repulsion term, the third term is the folded gaussian attraction term, and the fourth term is the Coulomb repulsion term.

We follow Refs. [21, 82] and use the parameters of $t_0 = -12.5$ MeV fm^{-1}, $t_3 = 8.8$ MeV fm^2, and interaction width $b = 2.0$ fm. For the Coulomb interaction, we set $\alpha = 1.0$ fm arbitrarily. With the Gaussian type single-particle wave function, each term of Hamiltonian can be written by Gaussian center z_{ai} as

$$\begin{aligned}\frac{\hbar^2}{2m}\int dx\tau_{ab}(x) &= \frac{\hbar}{2m}\sum_{i,j}\delta_{\sigma_i\sigma_j}\delta_{\tau_i\tau_j}e^{\frac{(z_{ai}^*-z_{bj})^2}{2}} \\ &\qquad \times \nu(1-(z_{ai}^*-z_{bj})^2)(B_{ab}^{-1})_{ji} \\ &= \frac{\hbar^2}{2m}\sum_{i,j}\nu(1-(z_{ai}^*-z_{bj})^2)(B_{ab})_{ij}(B_{ab}^{-1})_{ji},\end{aligned} \tag{4.17}$$

$$\frac{t_3}{3}\int dx\rho_{ab}^3(x) = \frac{t_3}{3\sqrt{3}}\frac{2\nu}{\pi}\sum_{ij}\sum_{kl}\sum_{mn} e^{-\frac{1}{3}(z_{(ij)}^2+z_{(kl)}^2+z_{(mn)}^2-z_{(ij)}z_{(kl)}-z_{(kl)}z_{(mn)}-z_{(mn)}z_{(ij)})} \times (B_{ab})_{ij}(B_{ab}^{-1})_{ji}(B_{ab})_{kl}(B_{ab}^{-1})_{lk}(B_{ab})_{mn}(B_{ab}^{-1})_{nm}, \tag{4.18}$$

$$\frac{t_0}{2}\int dx\rho(x)\int dx'\rho(x')\frac{b}{\sqrt{\pi}}e^{-\frac{(x-x')^2}{b^2}} = \frac{t_0 b}{2\sqrt{\pi}}\sqrt{\frac{\nu b^2}{1+\nu b^2}}\sum_{i,j}\sum_{i',j'} B_{ij}(B^{-1})_{ji}B_{i'j'}(B^{-1})_{j'i'}e^{-\frac{(z_{(ij)}-z_{(i'j')})^2}{4(1+\nu b^2)}}, \tag{4.19}$$

where $z_{(ij)} \equiv z_{ai} - z_{bj}$. Only the Coulomb term cannot be integrated analytically, thus it is integrated numerically in this calculation. In order to derive the time-dependent equation Eq. (4.1) for $z_a(t)$ and Eq. (4.2) for $f_a(t)$, evaluation of the derivative of $\langle\Psi|H|\Psi\rangle / \langle\Psi|\Psi\rangle$ with respect to $z_a^*(t)$ and $f_a^*(t)$ are required. We carry them out numerically by finite differentiation

$$\partial_{z_a^*}\frac{\langle\Psi|H|\Psi\rangle}{\langle\Psi|\Psi\rangle}(z_a^*) \simeq \frac{\frac{\langle\Psi|H|\Psi\rangle}{\langle\Psi|\Psi\rangle}(z_a^*+\delta z_a^*) - \frac{\langle\Psi|H|\Psi\rangle}{\langle\Psi|\Psi\rangle}(z_a^*-\delta z_a^*)}{2\delta z_a^*}, \tag{4.20}$$

$$\partial_{f_a^*}\frac{\langle\Psi|H|\Psi\rangle}{\langle\Psi|\Psi\rangle}(f_a^*) \simeq \frac{\frac{\langle\Psi|H|\Psi\rangle}{\langle\Psi|\Psi\rangle}(f_a^*+\delta f_a^*) - \frac{\langle\Psi|H|\Psi\rangle}{\langle\Psi|\Psi\rangle}(f_a^*-\delta f_a^*)}{2\delta f_a^*}. \tag{4.21}$$

Note that the derivatives are independent from the directions of δz_a^* and δf_a^* in the complex plane when the absolute values of δz_a^* and δf_a^* are small enough.

In the calculations shown below, we set the Gaussian width of $\nu = 0.5$ fm^{-2}. This value is determined in order that the internucleus potential at $x = 0$ evaluated in the frozen density approximation with a single Slater determinant [48] should becomes higher than the height of the Coulomb barrier. With the employed parameter, the barrier in the frozen density approximation is located at a relative distance R=7.68 fm with the height of 0.13 MeV as shown in Fig. 4.1.

The frozen density approximation is a method of approximating the potential surface by calculating the energy of two ground-state nuclei at different relative distances R. In this approximation, the two nuclei are assumed to be stationary and internal excitations are not taken into account. In this case, the energy of the nuclei placed at a distance R between the nuclei is $E(R)$, which is calculated by the following equation.

$$E(R) = 2V_0 - V_C(R_0) \tag{4.22}$$

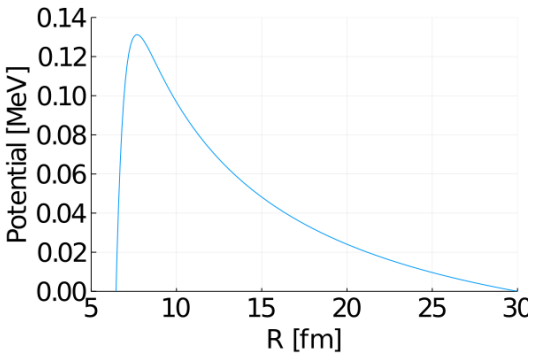

Figure 4.1: Internulear potential obtained by frozen density approximation. The Coulomb barrier with a height of 0.13 MeV is located at a relative distance R =7.68 fm.

where V_0 is the energy of a single isolated nucleus. $V_c(R_0)$ is the Coulomb potential at the distance R_0 between nuclei in the initial configuration used in the following calculation, and by subtracting this, the actual height of the Coulomb barrier felt by the nucleus can be estimated.

If the Coulomb barrier is larger than the internuclear potential, the wave packet crossing the Coulomb barrier is likely to fly to the other side, also crossing the internuclear potential. The reason for this is that the collision energy is not sufficiently converted to the energy of internal excitation under the assumption of identical Gaussian centers of ^{4}He single-particle wave function given here, and as a result, the relative motion between nuclei is not trapped. If there is a Slater determinant in which the relative motion between the nuclei is not trapped and the nuclei exit to the other side, there will be an overlap between a Slater determinant and a Slater determinant reflected by the Coulomb barrier, which will cause a problem when defining the transmission probability of the Coulomb barrier.

4.2.2 Trajectories

We first discuss the result of a superposition of two Slater determinants. One set of the Slater determinants has the initial positions of the α particles $x_0 = \pm 15.0$ fm with the initial relative momentum of $p_0 = \mp\sqrt{2\mu E}$ with $E = 0.113$ MeV, where μ is the reduced mass evaluated with the static calculation for a single α particle, while the other set of Slater determinant have $x_0 = \pm 15.1$ fm and $p_0 = \mp\sqrt{2\mu E}$ with $E = 0.100$ MeV. Fig. 4.2 shows the position of each Gaussian wave packet, $x(t) = \mathrm{Re}[z(t)]/\nu$, where Re[$z$] means the real part of z only the components with $x > 0$ are shown. In the case of Fig. 4.2, the Slater

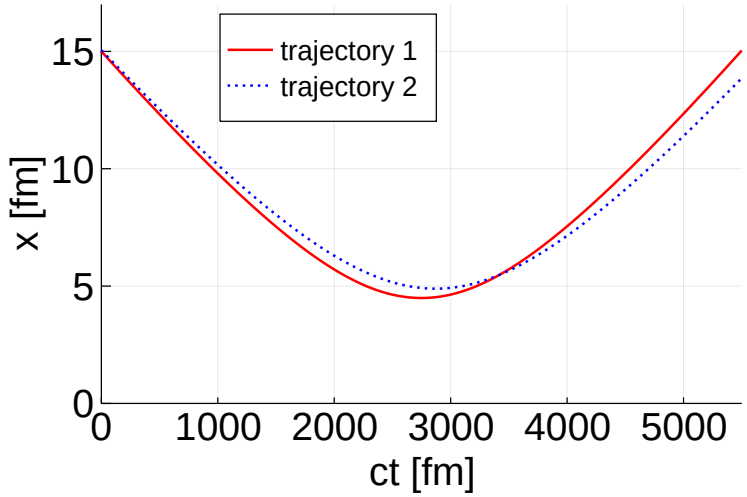

Figure 4.2: The trajectories of the right α particle in $\alpha + \alpha$ scattering in one dimensional space. The trajectories are obtrained with the antisymmetrized molecular dynamics with two different initial conditions. Since the two α particle are assumed to move symmetrically wth respect to $x = 0$, only the trajectories of the right α are shown. The solid line is obtained wiht the initial condition of initial potitions $x_0 = 30.0/2$ fm and initial energy of relative motion $E = 0.113$ MeV, while the dashed line is obtained with $x_0 = 30.1/2$ fm and $E = 0.100$ MeV. The interaction include a Gaussian + density-dependent zero-range nuclear interaction and a soft-core Coulomb interaction. The Coulomb barrier between the two α particles is located at $x = 3.84$ fm with the height of 0.13 MeV

determinants are evolved independently to each other with the AMD. Both of the trajectories are reflected at the barrier located at 3.84 fm because the initial energy is below the barrier for both the Slater determinants. Fig. 4.3 shows the result of the TDGCM with two Slater determinants, for which the initial conditions are taken to be the same as those in the independent TDHF calculations in Fig. 4.2. In this calculation, we initially take equal weights for the two Slater determinants, that is, $f_1 = f_2$. The average initial relative energy, $E_{\rm rel} \equiv \langle\Psi|H|\Psi\rangle / \langle\Psi|\Psi\rangle - 2E_{\rm g.s.}$, where $E_{g.s.}$ is the ground state energy of the particle. In this calculation $E_{\rm rel} = 0.099$ MeV, which is still below the Coulomb barrier. Nevertheless, it is clearly seen that one of the trajectories overcomes the barrier and trapped in internuclear potential, while the other trajectory is reflected at the barrier. This is in marked contrast to the TDHF case shown in Fig.4.2, in which both of the trajectories are reflected at the barrier. This result means that a finite tunneling probability

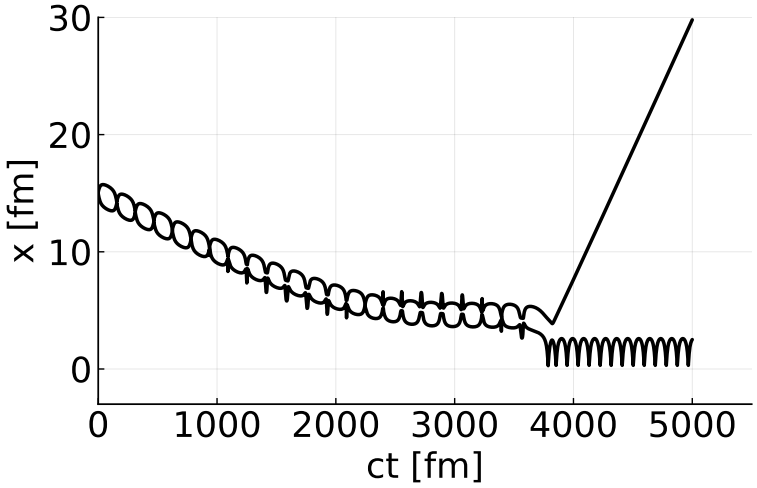

Figure 4.3: Same as Fig. 4.2, but the trajectories in this figure are obtained with the time-dependent generator coordinate method with the same initial conditions as Fig. 4.2.

of the Coulomb barrier is realized in the TDGCM even though that is zero in TDHF.

4.2.3 Tunneling probability

Figure 4.4 shows the time-evolution of the probabilities of each trajectory in the wave function. Here, the probabilities are defined as,

$$P_i(t) = \frac{|f_i|^2 \langle \Phi_i(t) | \Phi_i(t) \rangle}{\langle \Psi | \Psi \rangle}. \tag{4.23}$$

Notice that we plot only the long-time behavior, for which the overlap between the two Slater determinants is small, that is, $\langle \Phi_1(t) | \Phi_2(t) \rangle \sim 0$. The fraction for the transmitted trajectory becomes from 0.5 at t = 0 to 0.489 at t = ∞. This value might be identified with the tunneling probability.

How to describe quantum tunneling

The trajectories of the Slater determinants in the TDGCM shown in the previous subsection showed that one of the Slater determinants transmitted through the barrier, even though the initial energies of the two superposed Slater determinants were both lower than the barrier. However, in fact, the superposed Slater determinant, when viewed alone, still cannot proceed into

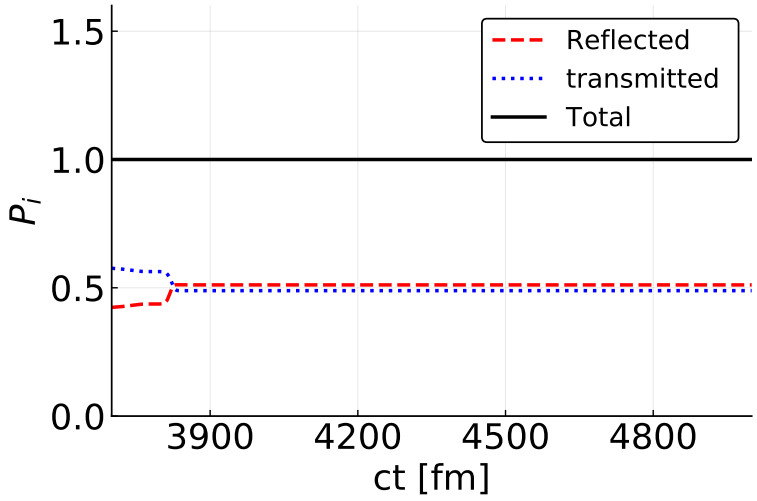

Figure 4.4: The time-evolution of the fractions of each Slater determinant shown in Fig. 4.2. The dashed and the doted lines show the reflected and the transmitted Slater determinant respectively. The solid line show the conservation of the total norm.

the classically forbidden region, i.e., the single Slater determinant does not tunnel in the same way as in quantum mechanics. The reason why TDGCM can describe the quantum tunneling effect is that the superposed Slater determinants exchange energy with each other, and the Slater determinants that cross the barrier borrow energy from the other Slater determinants, in a sense crossing the barrier classically.

In practice, it is difficult to define strictly the energy of a given Slater determinant in the superposition because of the overlap between Slater determinants, but as a measure, the energy defined by

$$E_a(t) = \frac{\langle \Phi_a(t)|H|\Phi_a(t)\rangle}{\langle \Phi_a(t)|\Phi_a(t)\rangle}. \tag{4.24}$$

is illustrated in Fig. 4.5, This is the energy of a single Slater determinant when the overlap between Slater determinants is almost zero.

As compared to the energies for the independent Slater determinants (see the thin dashed and dotted lines), the energy of one of the trajectories (the trajectory 1; the thick dashed line) increases while that of the other trajectory (the trajectory 2; the thick dotted line) decreases, even though the total energy of the system,

$$E_{\rm tot} = \frac{\sum_{ab} f_a^*(t) f_b(t) \langle \Phi_a(t)|H|\Phi_b(t)\rangle}{\sum_{ab} f_a^*(t) f_b(t) \langle \Phi_a(t)|\Phi_b(t)\rangle}, \tag{4.25}$$

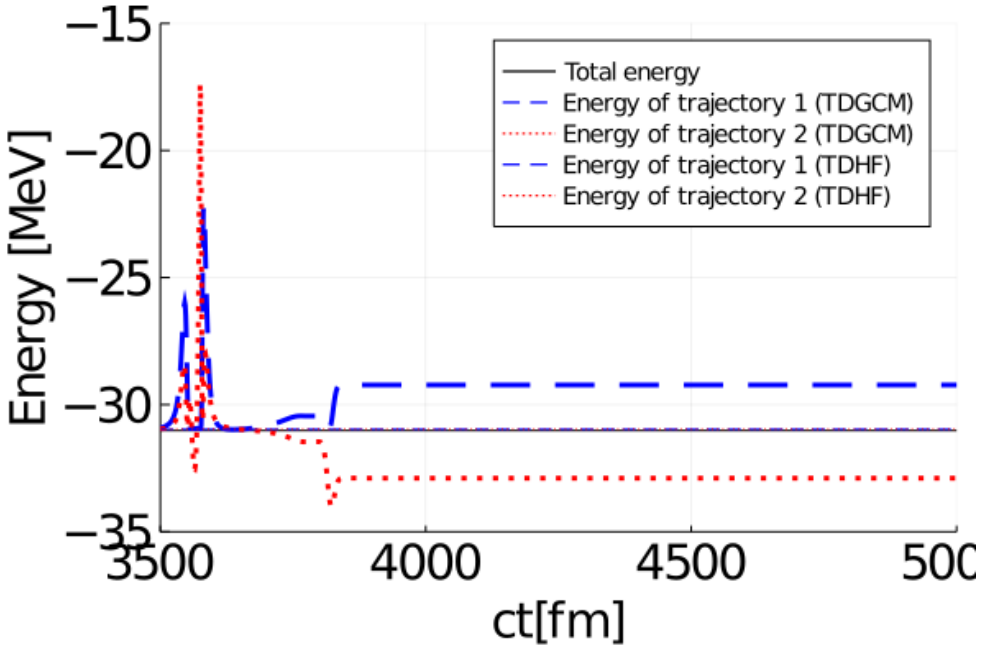

Figure 4.5: The time-evolution of the energy of each Slater determinant in the time-dependent generator coordinate method. The bold dashed and the dotted lines show that in the time-dependent generate coordinate method, and the thin dashed line(-30.95MeV) and the dotted line(-30.96MeV) show that in the AMD. While the total energy is conserved as shown by the solid line, the energy of each trajectory changes as a function of time in time-dependent generator coordinate method.

remains a constant at any time (see the solid line). Notice that the trajectory 1 corresponds to the reflected fraction in Fig. 4.4, while the trajectory 2 corresponds to the transmitted fraction in Fig. 4.4. At the time when the relative motion of the nucleus hits the Coulomb barrier ($ct \approx 3500$ [fm]), the diagonal enegies of the trajectories 1 and 2 appear to be increased, resulting in trajectory 2 crossing the barrier.

4.3 Application to collision of ^{4}He and the Gaussian external barrier

In the system treated in Sec. 4.2, it was shown qualitatively that TDGCM can describe the tunneling effect. However, in the collision of the two ^{4}He particles system, there were some problems to understand the TDGCM mech-

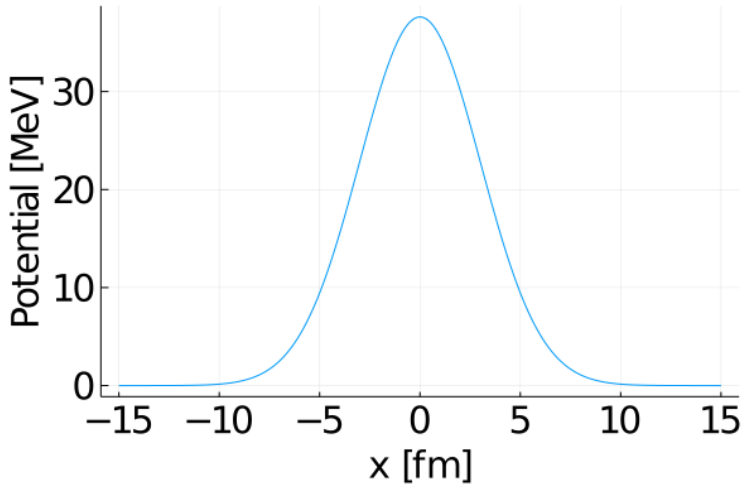

Figure 4.6: The potential barrier obtained by the frozen density approximation.

anism in more details. In high-energy collisions, for example, the nuclei that cross the Coulomb barrier slip through each other and fly to the other side. In this case, the trajectories reflected by the Coulomb barrier and the trajectories slipped through by the nuclei have an overlap, and this causes a practical problem that the penetration probability of the Coulomb barrier cannot be well defined. In addition, in the collision system, there are trajectories trapped by the internuclear potential and the nuclei keep vibrating, so the kinetic energy continues to change even in the final state, making it difficult to analyze the energy distribution in the final state. For these reasons, in this section, the above problem is avoided by using a system in which a ^{4}He particle collide with an external Gaussian barrier.

4.3.1 Setup

The interaction used in this section is as follows

$$V(x) = \sum_i v_i = \sum_i v_0 e^{-a_v x_i^2}, \tag{4.26}$$

where barrier height $v_0 = 80$ MeV and barrier width $a_v = 1$ [1/fm^{-2}], that is, each nucleon feels the same Gaussian potential. The potential barrier obtained by the frozen density approximation is shown in Fig. 4.6. As can be seen from this Fig. 4.6, the effective height of the potential barrier felt by the wave packet is not the original v_0, but a lower value of 37 MeV.

Here, the values of v_0 and a_v are chosen so that the tunneling probabilities with different collision energies can be calculated from 0 to 1 , which will be shown later. However, the qualitative behavior of the calculated results does not depend on the particular values of v_0 and a_v.

The matrix elements of the interaction in Eq. (4.26) can be written using the Gaussian center z_a as follows

$$\begin{aligned}\langle\Phi_a|V|\Phi_b\rangle &= \langle\Phi_a|\Phi_b\rangle \sum_{ij} \langle v_i \phi_i^a | \phi_j^b\rangle \, (B^{-1})_{ji} \\ &= \langle\Phi_a|\Phi_b\rangle \sum_{ij} v_0 \sqrt{\frac{2\nu}{a_v+2\nu}} e^{\frac{\nu(z_{ai}^*+z_{bj})^2}{a_v+2\nu} - (z_{ai}^{*2}+z_{bj}^2)} (B_{ab}^{-1})_{ji}. \end{aligned} \tag{4.27}$$

This section also uses the approximation that the nucleon Gaussian centers in ^{4}He are identical, and we use the Gaussian width of $\nu = 0.142$ fm^{-2} which minimizes the energy of ground state of ^{4}He with the Hamiltonian which is used in Eq. (4.14). The derivatives of $\mathcal{H}$ with respect to z_a and f_a in the equations of motion Eqs. (4.1) and (4.2) are performed by numerical differentiation as in the case of Sec. 4.2.

In the calculations that follow, the initial conditions are prepared according to the following procedures.

- Construct TDGCM wave function around the origin,

$$|\Psi(x_1, x_2, ...; t=0)'\rangle = \sum_a f_a(t=0) \, |\Phi_a(x_1, x_2, ...; t=0)\rangle \, , \tag{4.28}$$

  where the generator coordinate a are the initial center-of-mass position x_a and initial center-of-mass momentum k_a of the Slater determinant. Given such x_a and k_a, the Gaussian center z_a' of each Slater determinant follows from the relation in Eq. (4.12)

$$z_a' = \sqrt{\nu} x_a + \frac{k_a}{2\sqrt{\nu}}. \tag{4.29}$$

- Then translate the TDGCM wave function to the potision $x = x_{\rm CM0}$ and accelerate it towards the barrier with the momentum $k = k_{\rm CM0}$,

$$|\Psi(x_1, x_2, ...; t=0)\rangle = e^{-k_{\rm CM0} x} \, |\Psi(x_1 - x_{\rm CM0}, x_2 - x_{\rm CM0}, ...; t=0)'\rangle \, , \tag{4.30}$$

  that is, this corresponds to a transformation of z_a as follows

$$z_a = z_a' + \sqrt{\nu} x_a + \frac{k_a}{2A\sqrt{\nu}}, \tag{4.31}$$

  for all a.

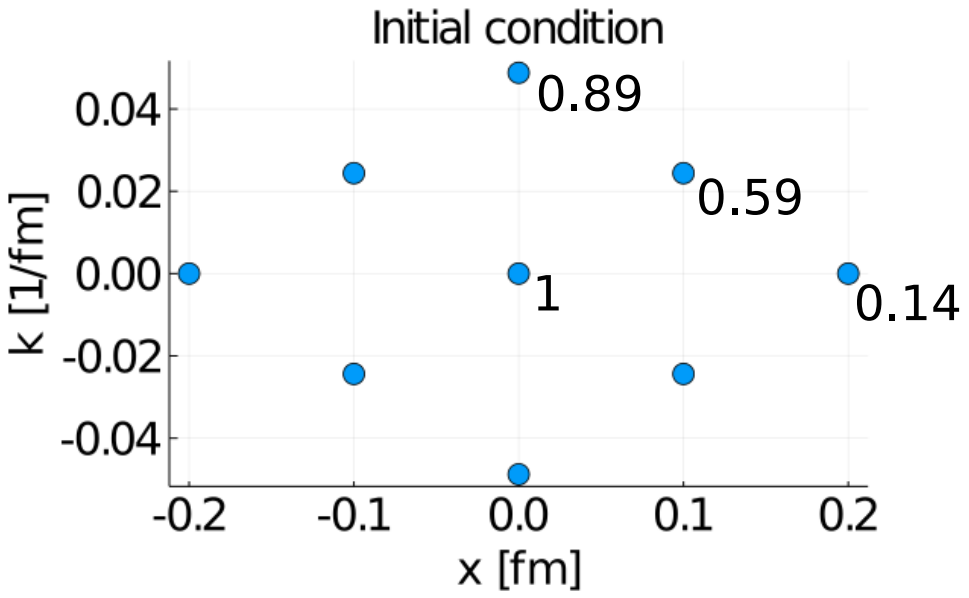

Figure 4.7: The initial center-of-mass position and momentum of nine Slater determinants. Each blue dots represent the each Slater determinants respectively, and the number besides the blue dots show the initial weight function for each Slater determinant. The Slater determinants are placed symmetrically with respect to $x = k = 0$ in phase space, and initial weight is distributed by Gaussian function $f(0) = e^{(-k^2/2\sigma_k^2)} e^{(-x^2/2\sigma_x^2)}$ where $\sigma_k = 0.1$ fm^{-1} and $\sigma_x = 0.1$ fm

4.3.2 Trajectories

First, we discuss the trajectories obtained with nine Slater determinants. The generation coordinates used in the calculation are shown by the blue dots in Fig. 4.7. The initial values of the corresponding weights f are indicated by the numbers beside the blue dots in Fig. 4.7. The initial values of center-of-mass momentum and center-of-mass position given to the Slater determinant were chosen arbitrarily under the condition that the Slater determinants have sufficient overlap with each other in phase space. The weights f are chosen according to a Gaussian distribution, represented by $f = e^{-\frac{x^2}{2\sigma_x^2}} e^{\frac{k^2}{2\sigma_k^2}}$. It can be interpreted that the wave function of the many-body Gaussian distribution is represented by sampling the Slater determinant at nine points. The schematic picture is shown in Fig. 4.8. If the distribution of the weights f does not change, the calculation result will not change no matter what Slater determinant is prepared. After constructing the TDGCM wave function $|\Psi'\rangle$ in Eq. 4.28 with the above initial paramters, the entire wave

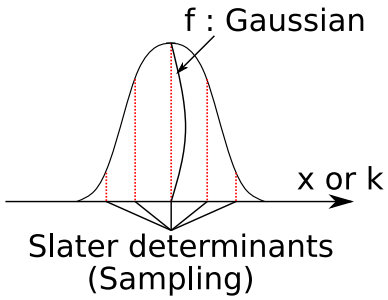

Figure 4.8: Schematic picture of choosing several Slater determinants. The initial wave packet is determined by the distribution of the weight function f, and the Slater determinants weighted by f represents the wave packet.

function is translated to the position $x_0 = 15$ fm and boosted with the several momenta to create the initial state of the calculation. The initial potision $x_0 = 15$ fm is chosen so that the wave function and the barrier loceted at $x = 0$ have an overlap small enough to ignore in the initial state. The results with $k_0 = 1.67\text{fm}^{-1}$ are representative of the results calculated with several different initial momenta.

The resulting trajectories are shown in Fig. 4.9 and Fig. 4.10. Fig. 4.9 shows the time evolution of each of the prepared SDs independently in AMD. x is the center of the Gaussian function representing the Slater determinant, which is also the center of the ^{4}He particle. All the trajectories are reflected by the Gaussian barrier at $x = 0$ for the given initial momentum.

On the other hand, Fig. 4.10 shows the results of TDGCM calculation using the prepared Slater determinants and the weights f as the initial conditions. As in the case shown in Chap. 4.2, the results of the TDGCM calculation differ from the independent AMD calculation (see Fig. 4.10) in that three trasmitted Slater determinants can be seen. Here, we define the trajectories that cross the barrier and go to the x<0 region as the transmitted trajectories. This difference, as in Chap. 4.2, is an evidence for that TDGCM describes a tunneling effect that was not possible with TDHF or AMD.

The energy E written at the top of Fig. 4.10 is defined as the center-of-mass kinetic energy after boosting the entire wave function minus that before boosting.

$$\frac{\langle\Psi|T_{\text{CM}}|\Psi\rangle}{\langle\Psi|\Psi\rangle} - \frac{\langle\Psi'|T_{\text{CM}}|\Psi'\rangle}{\langle\Psi'|\Psi'\rangle}, \tag{4.32}$$

where $|\Psi\rangle$ and $|\Psi'\rangle$ are defined in Eqs. (4.28) and (4.30) respectively.

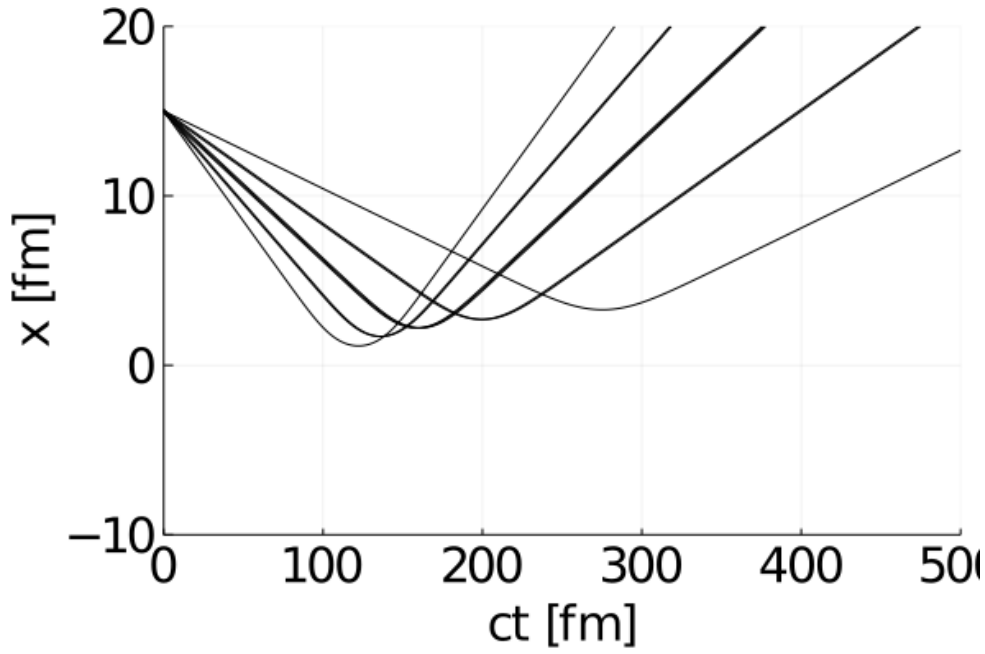

Figure 4.9: The trajectories of α particle in α scattering by external barrier in one dimension obtained with the AMD with nine different initial conditions shown in Fig. 4.7. The all Slater determinants are boosted with $k = 1.67$ fm^{-1}. There is no interaction between nucleons, and nucleons only feel the same external barrier. The external barrier located at $x = 0$ with effective height of 37.6 MeV.

The center-of-mass kinetic energy operator $T_{\rm CM}$ is defined as

$$T_{\rm CM} = \frac{-\hbar^2}{2Am_N}\partial_R^2, \tag{4.33}$$

where m_N is the nucleon mass and $\partial^2_{R_G}$ is the differential operator with respect to the center of mass position $R = \sum_i x_i/A$. The matrix elements of $T_{\rm CM}$ can be written in terms of the Gaussian centers z as follows

$$\begin{aligned}
\langle\Phi_a|\hat{T}_{CM}|\Phi_b\rangle &= \langle\Phi_{{\rm CM}a}\Phi_{\rm int}|\hat{T}_{CM}|\Phi_{{\rm CM}b}\Phi_{\rm int}\rangle \\
&= \langle\Phi_{{\rm CM}a}|\hat{T}_{CM}|\Phi_{{\rm CM}b}\rangle\,\langle\Phi_{\rm int}|\Phi_{\rm int}\rangle \\
&= -\frac{\hbar^2}{2Am_N}\,\langle\Phi_{{\rm CM}a}|\partial_R^2|\Phi_{{\rm CM}b}\rangle\,\langle\Phi_{\rm int}|\Phi_{\rm int}\rangle \\
&= -\frac{\hbar^2 A\nu}{2m_N}\left((z_a^* - z_b)^2 - \frac{D}{A}\right)\langle\Phi_a|\Phi_b\rangle\,,
\end{aligned} \tag{4.34}$$

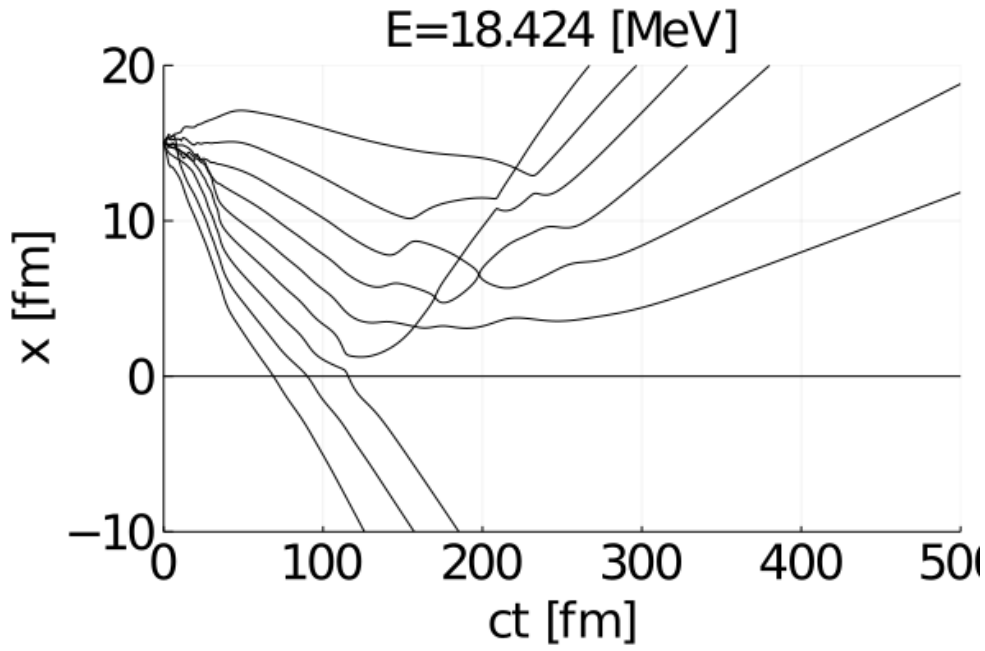

Figure 4.10: Same as Fig. 4.9, but obtained with the time-dependent generator coordinate method with the same initial conditions.

where D is the number of dimensions, which is 1 in the present calculation. The center-of-mass part $\Phi_{\rm CM}$ and the interior part $\Phi_{\rm int}$ of the Slater determinant can be written as follows

$$\Phi_{{\rm CM}a} = e^{-A\nu\left(R-\frac{z_{{\rm CM}a}}{\sqrt{\nu}}\right)^2}, \tag{4.35}$$

$$\Phi_{\rm int} = \sum_\sigma (-)^\sigma \left\{ e^{-\nu\left(x_1-R-\frac{z_{\sigma_1}-z_{{\rm CM}a}}{\sqrt{\nu}}\right)^2} e^{-\nu\left(x_2-R-\frac{z_{\sigma_2}-z_{{\rm CM}a}}{\sqrt{\nu}}\right)^2} \cdots \right\}, \tag{4.36}$$

where $z_{{\rm CM}a} = \sum_i z_{ai}/A$, and $\sum_\sigma (-)^\sigma$ means antisymmetrization for particle exchange. Here we used the fact that the Slater determinant can be divided into a center-of-mass part $|\Phi_{\rm CM}\rangle$ and an intrinsic part $|\Phi_{\rm int}\rangle$. Note that since the center-of-mass position and the center-of-mass momentum are taken as the generating coordinates, the intrinsic state of each Slater determinant $|\Phi_a\rangle$ is the same regardless of the generating coordinates. The energy written in Fig. 4.10 is $E = 18.424$ MeV , which is lower than the barrier height of 37.6 MeV obtained by the frozen density approximation.

Next, we discuss the time evolution of the center-of-mass wave function

defined as

$$\Psi_{\rm CM}(R) = \sum_a f_a \Phi_{{\rm CM}a}(R) \tag{4.37}$$

$$= \sum_a e^{-A\nu\left(R - \frac{z_{{\rm CM}a}}{\sqrt{\nu}}\right)^2}. \tag{4.38}$$

First, the time evolution of the density distribution $\rho_{\rm CM}(R) = |\Psi_{\rm CM}(R)|^2$ for the center-of-mass wave function is shown in Fig. 4.11 At time $ct = 50$ fm, no collision has occurred yet, so the wave packet has the same Gaussian shape as in the initial state. At time $ct = 100$ fm, when the collision occurs, the wave packet is scattered and its shape is disordered. After the collision, the wave function is divided into the wave packets that crosse the barrier and the wave packets that are reflected by the barrier, and the spatial overlap between the two becomes zero at $ct \to \infty$.

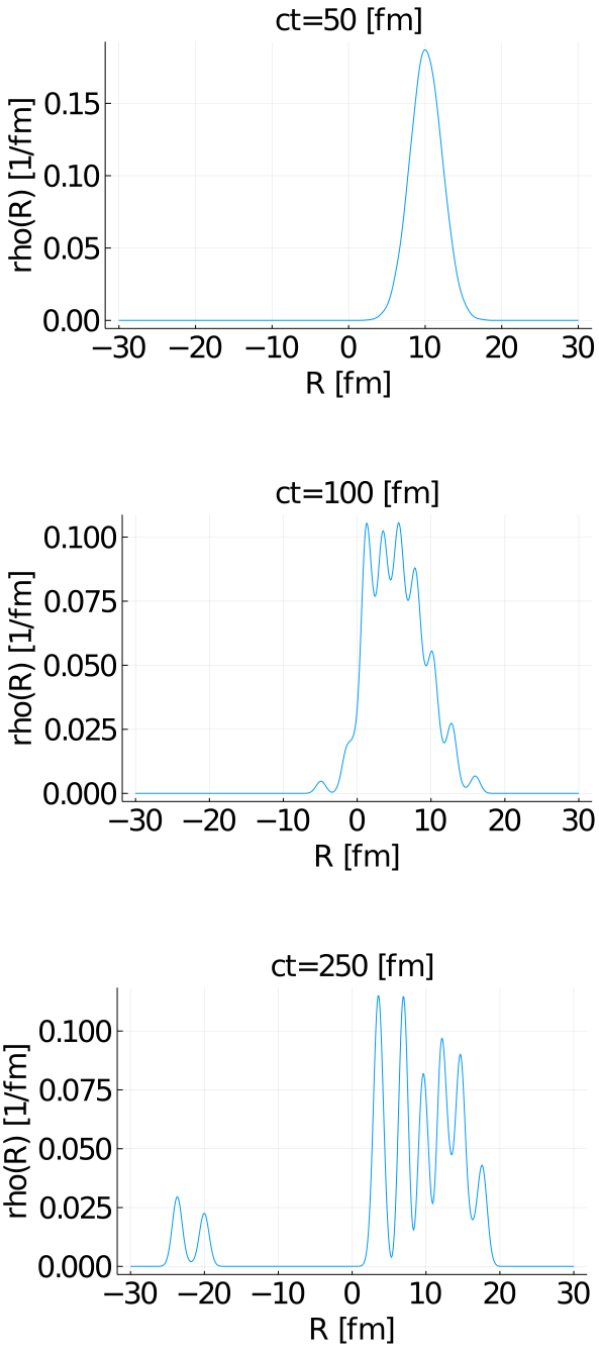

Figure 4.11: Snapshots of the density function $\rho_{\mathrm{CM}}(z) = |\Psi_{\mathrm{CM}}(z)|^2$ at several times. The vertical axis is the density function and the horizontal axis is the center-of-mass coordinate R. In the TDGCM calculation, a collision between ^{4}He and the barrier occur at around time $ct = 70$ fm

4.3.3 Energy dependence of the tunneling probability

In this section, we discuss the collision energy dependence of the transimission probability. The definition of transmission probability is an extension of Eq. (4.23) and is defined as follows

$$P_{\rm trans} = \frac{\sum_{a,b:\text{transmitted}} f_a^* f_b \langle \Phi_a | \Phi_b \rangle}{\langle \Psi | \Psi \rangle}, \tag{4.39}$$

that is, $P_{\rm trans}$ is defined as the norm of the transmitted wave packets relative to the norm of the overall wave function. The calculated transmission probabilities for various boost energies to the overall wave function are shown in Fig. 4.12. The blue line represents the result of the TDGCM calculation, and the orange line is the independent AMD result for comparison. The blue line show the transmission probability where the Slater determinants and their weights evolve in time by TDGCM. The orange line show also the transmission probability, but each Slater determinant independently evolve in time by AMD and their weights are fixed in time. The transmission probability calculated by each method is expressed in the following equation

$$P_{\rm TDGCM} = \frac{\sum_{a,b:\text{transmitted}} f_a^*(t_{\rm end}) f_b(t_{\rm end}) \langle \Phi_a(t_{\rm end}) | \Phi_b(t_{\rm end}) \rangle}{\langle \Psi(t_{\rm end}) | \Psi(t_{\rm end}) \rangle} \text{ (for blue line)}, \tag{4.40}$$

$$P_{\text{independent AMD}} = \frac{\sum_{a,b:\text{transmitted}} f_a^*(t=0) f_b(t=0) \langle \Phi_{a,\rm AMD}(t_{\rm end}) | \Phi_{b,\rm AMD}(t_{\rm end}) \rangle}{\langle \Psi_{\rm AMD}(t_{\rm end}) | \Psi_{\rm AMD}(t_{\rm end}) \rangle} \text{ (for orange line)}, \tag{4.41}$$

where $t_{\rm end}$ is a large time enough for the overlap between wave packets separated by the barrier to become negligible. The first thing to notice is that the transmission probability is increased in the blue line compared to the orange line at energies below the barrier. In particular, the TDGCM results shows finite transmission probabilities even for energies at which all the AMD trajectories are reflected by a barrier, as shown by the orange line.

Also, at energies above the barrier, the transmission probability is decreased, unlike the AMD results. This decrease in the transmission probability at high energies is also seen in quantum mechanics, and from this point of view, the TDGCM can be said to mimic quantum mechanics.

4.3.4 Time variation of the transmission probability

In this subsection, we investigate how the TDGCM wave function penetrates the barrier from the time variation of the transmission probability shown in

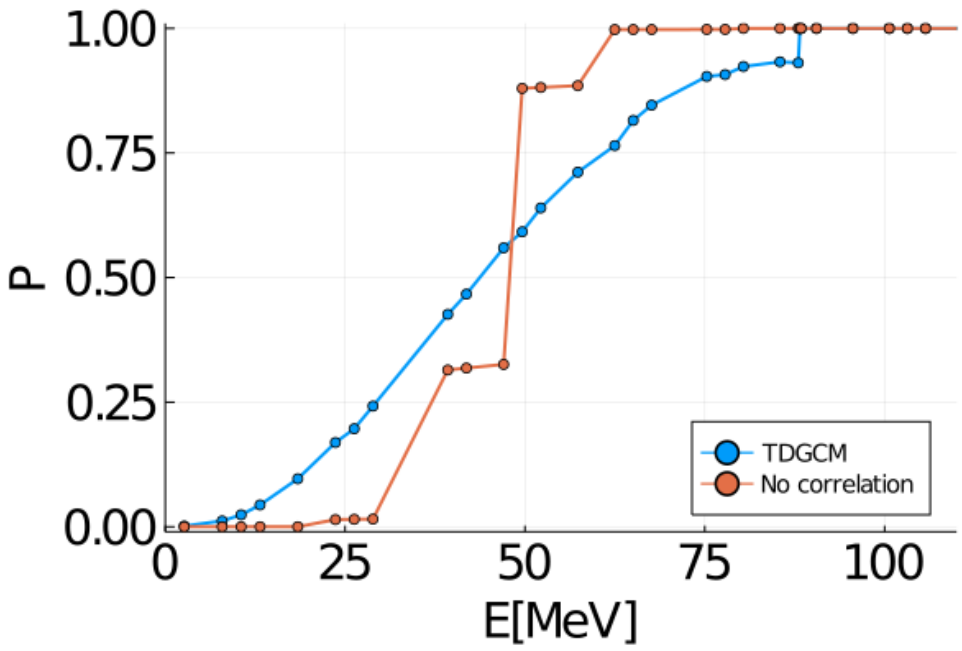

Figure 4.12: Dependence of transmission probability on collision energy. The vertical axis is the barrier transmission probability and the horizontal axis is the energy defined in Eq. (4.39). The blue curve shows the result of the TDGCM calculation, while the orange curve shows the result obtained by an independent AMD calculations. Although the same initial Slater determinant and initial weights are used at each point of the two resultant curves, TDGCM calculates the time evolution by superposing the weighted initial Slater determinants, whereas the independent AMD calculation evolves each given Slater determinant independently in AMD, and calculates the transmission probability of Eq. (4.39).

Fig. 4.13. This calculation is performed under the same conditions as those used to obtain the results in Fig. 4.10. The transmission probability shown in Fig. 4.13 is defined by Eq. 4.39, and is calculated at each time using the Slater determinants, which are known to be transmitted in the final state. What is characteristic about this time dependence in the transmission probability is that it only changes significantly upon impact with the barrier. In the trajectories shown in Fig. 4.10, the collision with the barrier occurs at $ct = 70 - 150$ fm, and it is during this period that most of the changes in the weights between the Slater determinants take place. When the overlap between the transmitted Slater determinant and the Slater determinant reflected by the barrier disappears, the weight transition also disappears.

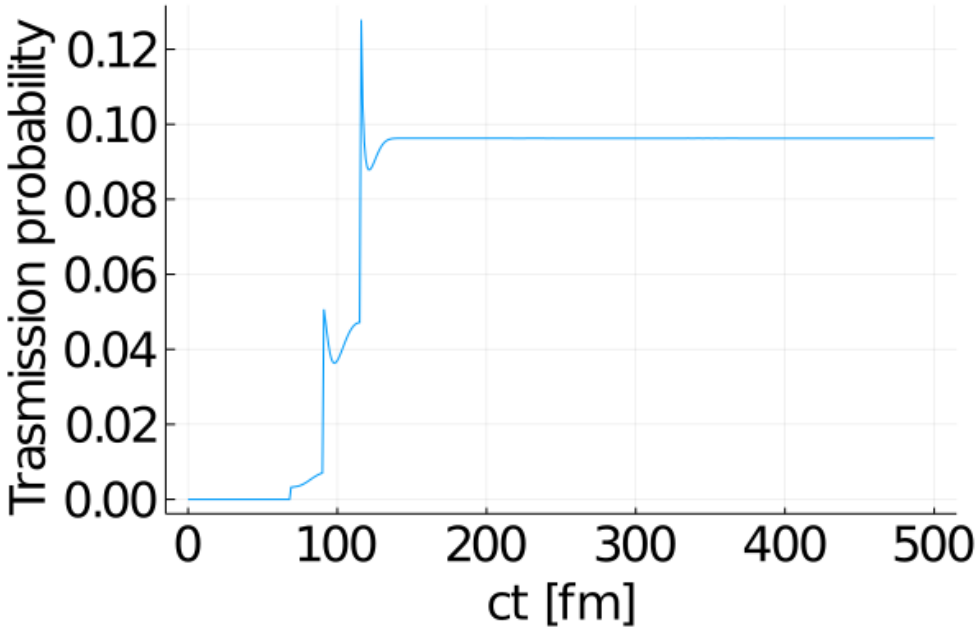

Figure 4.13: Time evolution of transmission probability. The kinetic energy of initial state $E = 18.424$ MeV, which is same as one in Fig. 4.10. The transmission probability is defined as Eq. (4.39). The weight transfer to the transmitted component starts when the TDGCM wave packet touches the barrier ($ct \approx 80$ [fm]), and the weight transfer is completed when the wave packet is completely split ($ct \approx 120$ [fm]).

This transition of the weights between the Slater determinants at the time of collision means that the TDGCM wave packet imitates the splitting of the quantum mechanical wave packet upon hitting the barrier, and the time variation of the weights is thought to create the smooth energy dependence of the transmission probability shown by the blue curve in Fig. 4.12.

4.3.5 Calculation using other sample points

We explained that the way to take the Slater determinants shown in the Fig. 4.7 is to sample a few points of the wave packet given by the weight f. Here we show that the resulting energy dependence of the transmission probability is independent of the sample points, although the sample points can be taken arbitrarily as long as there is enough overlap between the Slater determinants. The sample points used are shown in the Figs. 4.14, 4.15 and 4.16.

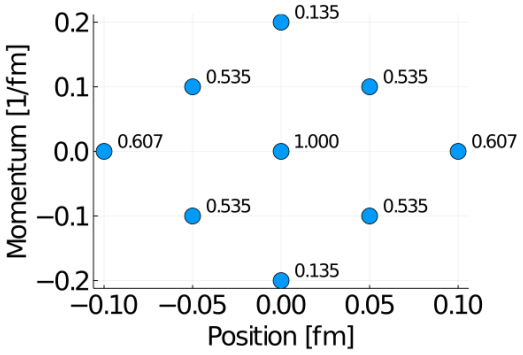

Figure 4.14: First sample of the initial center-of-mass position and momentum given to each Slater determinant, and the weights on those Slater determinants.

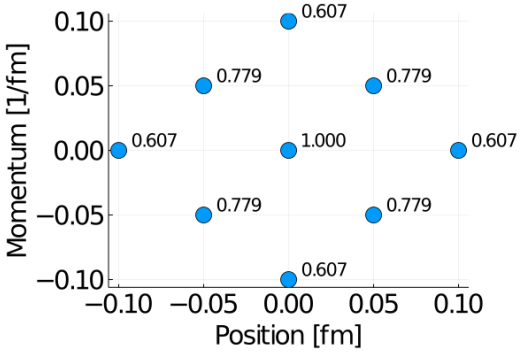

Figure 4.15: Second sample.

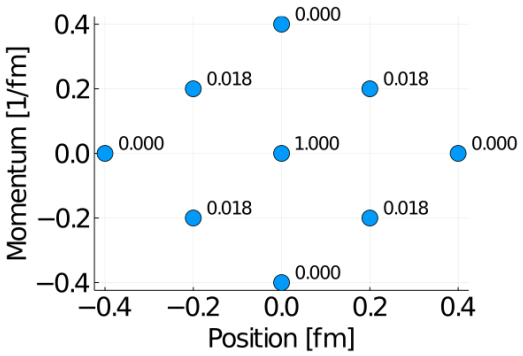

Figure 4.16: Third sample.

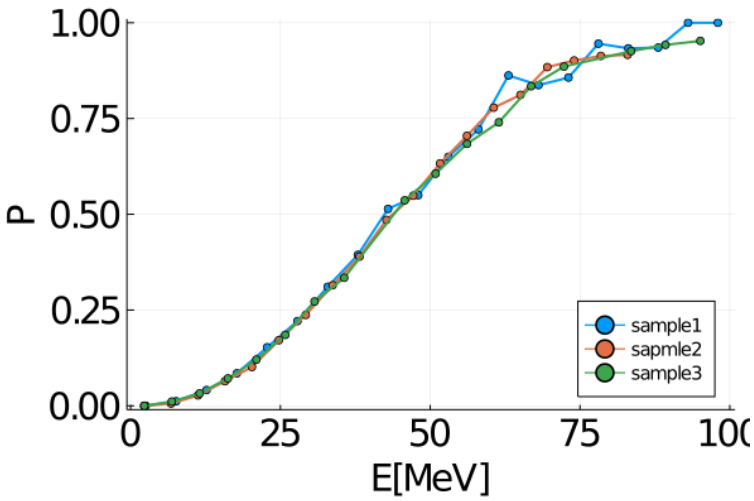

Figure 4.17: Energy dependence of the barrier transmission probability calculated using three samples with different initial Slater determinants. The definitions of the vertical and horizontal axes are the same as in Fig. 4.12 In the energy region below the height of the barrier, there is almost no difference in the results. In the energy region above the height of the barrier, there is no significant difference, although there is some fluctuation.

As in the Fig. 4.7, the blue points in the phase space represent the initial values of the center-of-mass position and momentum of each Slater determinant, and the numbers above the points are the weights f for each Slater determinant. The results of calculating the energy dependence of the transmission probability for each of the above three choices of Slater determinants are shown in the Fig. 4.17. As shown in this figure, we can see that using samples with different Slater determinants as the initial conditions does not change the results much, especially at energies below the barrier.

4.4 Application to collision of ^{4}He+^{4}He in three-dimension

In the Secs. 4.2 and 4.3, it is shown that the tunneling effect can be described in the TDGCM framework, and we have been defined the transimtting probability as the function of collision energy in the case of collision of ^{4}He particle and an external barrier. However, TDGCM still has many points to improve in order to describe the real nuclear reaction. In this section, we will extend the TDGCM to three-dimensional one, and show the result of collision of two

^{4}He particles in three-dimensional space. This extension is essential to the application of TDGCM to realistic cases.

In the follwing calculation, we use the Volkov No.1 interaction [103] between all nucleons,

$$V_V(r) = (W + MP_\sigma P_\tau)(V_a e^{-\vec{r}^2/r_a^2} + V_r e^{-\vec{r}^2/r_r^2}), \tag{4.42}$$

where $\vec{r}$ is the relative position vector of two interacting nuclei, and $V_a e^{-\vec{r}^2/r_a^2}$ and $V_r e^{-\vec{r}^2/r_r^2}$ are attractive and repulsive potential respectively. The P_σ and P_τ are the spin and isospin exchange operators, respectively. The values of parameters are set as $M = 0.56$,$W = 0.44$,$r_a = 1.6$ fm,$r_r = 0.82$ fm,$V_a = -83.34$ MeV and $V_r = 144.86$ MeV. In addition, the Coulomb interaction between each protons,

$$V_C(r) = \frac{e^2}{|\vec{r}|}, \tag{4.43}$$

is included. The matrix elements of these interactions can be written as a function of the Gaussian center $\vec{z}$ as follows

$$\begin{aligned}
\langle \Phi_a | V_V | \Phi_b \rangle = & \sum_{ijkl} (B^{ab})^{-1}_{ik} (B^{ab})^{-1}_{jl} \\
& \Big[(W w_{ijkl} - M w_{ijlk}) B^{ab}_{ik} B^{ab}_{jl} \\
& \times \Big\{ V_a \left(\frac{\nu}{a_a + \nu} \right)^{\frac{3}{2}} \exp\left(-\frac{a_a}{4(a_a+\nu)} (\vec{z}_i^{a*} - \vec{z}_j^{a*} + \vec{z}_k^{b} - \vec{z}_l^{b})^2 \right) \\
& + V_r x \left(\frac{\nu}{a_r x + \nu} \right)^{\frac{3}{2}} \exp\left(-\frac{a_r x}{4(a_r x+\nu)} (\vec{z}_i^{a*} - \vec{z}_j^{a*} + \vec{z}_k^{b} - \vec{z}_l^{b})^2 \right) \Big\} \\
& - (W w_{ijlk} - M w_{ijkl}) B^{ab}_{il} B^{ab}_{jk} \\
& \times \Big\{ V_a \left(\frac{\nu}{a_a + \nu} \right)^{\frac{3}{2}} \exp\left(-\frac{a_a}{4(a_a+\nu)} (\vec{z}_i^{a*} - \vec{z}_j^{a*} + \vec{z}_l^{b} - \vec{z}_k^{b})^2 \right) \\
& + V_r x \left(\frac{\nu}{a_r x + \nu} \right)^{\frac{3}{2}} \exp\left(-\frac{a_r x}{4(a_r x+\nu)} (\vec{z}_i^{a*} - \vec{z}_j^{a*} + \vec{z}_l^{b} - \vec{z}_k^{b})^2 \right) \Big\} \Big],
\end{aligned} \tag{4.44}$$

$$\begin{aligned}
\langle \Phi_a | V_C | \Phi_b \rangle = & \frac{2}{\sqrt{\pi}} \sum_{ijkl} B^{ab}_{ik} B^{ab}_{jl} (B^{ab})^{-1}_{ik} (B^{ab})^{-1}_{jl} \\
& \int_0^\infty d\gamma \left(\frac{\nu}{\gamma^2 + \nu} \right)^{\frac{2}{3}} \exp\left(-\frac{\gamma^2}{\gamma^2+\nu} \frac{(\vec{z}_i^{a*} - \vec{z}_j^{a*} + \vec{z}_k^{b} - \vec{z}_l^{b})^2}{4} \right),
\end{aligned} \tag{4.45}$$

where $a_a = 1/r_A, a_r = 1/r_r$ and w_{ijkl} is defined as

$$w_{ijkl} = \delta s_i s_k \delta s_j s_l \delta \tau_i \tau_k \delta \tau_j \tau_l, \tag{4.46}$$

where s and τ indicate the direction of the spin and isospin.

For simplicity, we have assumed the head-on collision, that is, the relative motion of the two ^{4}He particles is restricted to the z-axis which is the collision axis. we have also assumed that the two ^{4}He particles move symmetricaly with respect to $x = 0$. Other assumptions, the fixed spin, isospin wave fuctions, the fixed Gaussian width ν, and using the common Gaussian center z for four nucleons in ^{4}He are the same as in Secs. 4.2 and 4.3. The value of fixed Gaussian width $\nu = 0.58$ fm^{-2} is used so that the energy of ^{4}He is minimized with the interactions in Eqs. (4.42) and (4.43) using the AMD calculation.

4.4.1 Trajectories

Firstly, the trajectories of Slater determinants which represent the two ^{4}He movement are shown in Fig. 4.18 and Fig. 4.19. The trajectories of the Slater determinants are shown in Fig. 4.18 and Fig. 4.19 are time evolved with AMD independently and with TDGCM, respectively. The initial wave packet for the sysytem with the two ^{4}He particles are prepared by the following two steps:

- Construct a wave function around the origin

$$|\Psi(x, t = 0)'\rangle = \sum_a f_a(t = 0) \, |\Phi_a(x, t = 0)\rangle \, . \tag{4.47}$$

- Translate it to the position $x = x_0$ and boost with the momentum $k = -k_0$

$$|\Psi(x_0, t = 0)\rangle = e^{-ik_0 x} \, |\Psi(x - x_0, t = 0)'\rangle \, . \tag{4.48}$$

  Now, from the symmetry of the ^{4}He particles motion assumed above, $x = -x_0$ and $k = -k_0$ are given for the other ^{4}He particle on the other side.

The translate and the boost are written in terms of Gaussian center z as

$$z' = z + \sqrt{(}\nu) x_0 - i \frac{k_0}{2A\sqrt{\nu}}. \tag{4.49}$$

In the following calculation, we use the initial positions $x_0 = -0.5, 0.5$ fm and initial momenta $k_0 = -0.01, 0.01$ fm^{-1} for the Slater determinants $|\Phi_a(x, t = 0)\rangle$, and the whole wave packet $|\Psi'\rangle$ is translated to $x_0 = 15$ fm, and boosted with the momentum $k_0 = 0.36$ fm^{-1}.

Even though the initial conditions for the calculations shown in Fig. 4.18 and Fig. 4.19 are the same, the trajectories in the two figures are markedly different. Because of the assumption of head-on collision, the dynamics of the system is restrected on the z-axis, so now we focus only z-component z_z of the three-dimensional position $\vec{z} = (z_x, z_y, z_z)$. The $z_{z,rel.}$ in the figures corresponds to the distance between ^{4}He particles which is equals to two times potision of the right ^{4}He particle.

Fig. 4.18 shows the result of independent AMD calculation with two different initial Slater determinants where both the trajectories are reflected by the barrier. On the other hand, one of the trajectories of the Slater determinant with TDGCM shown in Fig. 4.19 overcomes the internuclear Coulomb barrier and is trapped by the nuclear attractive potential (the vibrating curve around the $z_z = 0$). This result is similar to the result of one-dimensional collision of two ^{4}He particles presented in Sec. 4.2. The similarity of the result of the one-dimensional and the three-dimensional calculations indicates that the TDGCM framework works in the three-dimensional space with the effective interactions for three-dimension, the Volkov No.1 interaction and the Coulomb interaction, which are widly used in exsisting AMD calculation.

4.4.2 Problems in TDGCM

In this section, we summarize and discuss the currently known issues in TDGCM. The first major problem is the large computational cost. We have introduced the following approximations.

- Use of a Gaussian single-particle wave function
- Matching the Gaussian centers of the nucleons in He
- Fixing the spin and isospin wave functions
- Fixing the Gaussian width of the single-particle wave function
- Assumption of head-on collision (three-dimensional calculation)

Under these approximations, the calculation of ^{4}He+^{4}He collisions in three dimensions takes about 30 minutes using a workstation (Intel Xeon E5-26909 v4). Note that in the TDGCM calculation, the process of calculating the matrix elements of the Hamiltonian like Eqs. (4.14),(4.28),(4.44) and (4.45)

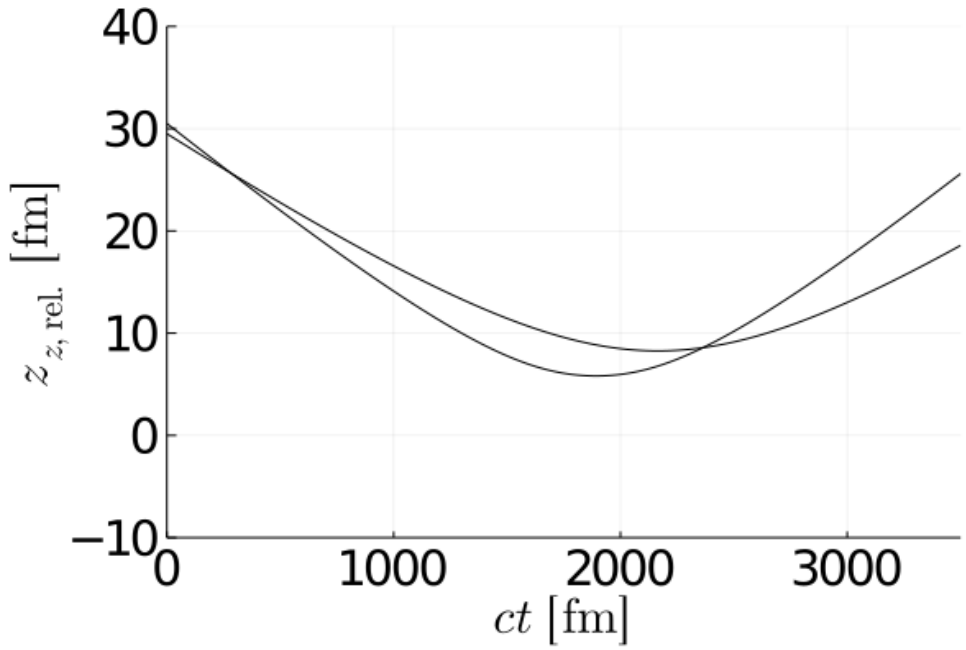

Figure 4.18: Trajectories of the center-of-mass position of the Slater determinants. The Slater determinants are independently time-evolved by AMD. Both of Slater determinants are reflected by the Coulomb barrier which is located at $z_{z,\mathrm{rel.}} = 6.6$ [fm].

is currently the most computationally expensive, and this computational cost increases with N^2 for N degrees of freedom. For example, if we exclude the head-on collision assumption in the three-dimensional calculation, the number of degrees of freedom to consider increases by a factor of three, but the cost of calculating the matrix element of the Hamiltonian increases by a factor of nine. Also, if we allow the Gaussian centers inside ^{4}He to move separately, the degrees of freedom will increase by a factor of four, and the computational cost of the Hamiltonian will increase by a factor of sixteen.

A different problem is the computational instability caused by the non-orthogonal nature of the Slater determinants. In TDGCM, several Slater determinants are superposed, but they are evolved in time and may become linearly dependent after some times. If the superposed Slater determinants become linearly dependent, the time evolution of the Slater determinants is not uniquely determined, and instability occurs in the calculation. In the case of a strictly linear dependence, the instability is certain to occur, but even in the case of a numerically close linear dependence, the calculation becomes unstable and the energy conservation is somewhat violated in our calculation.

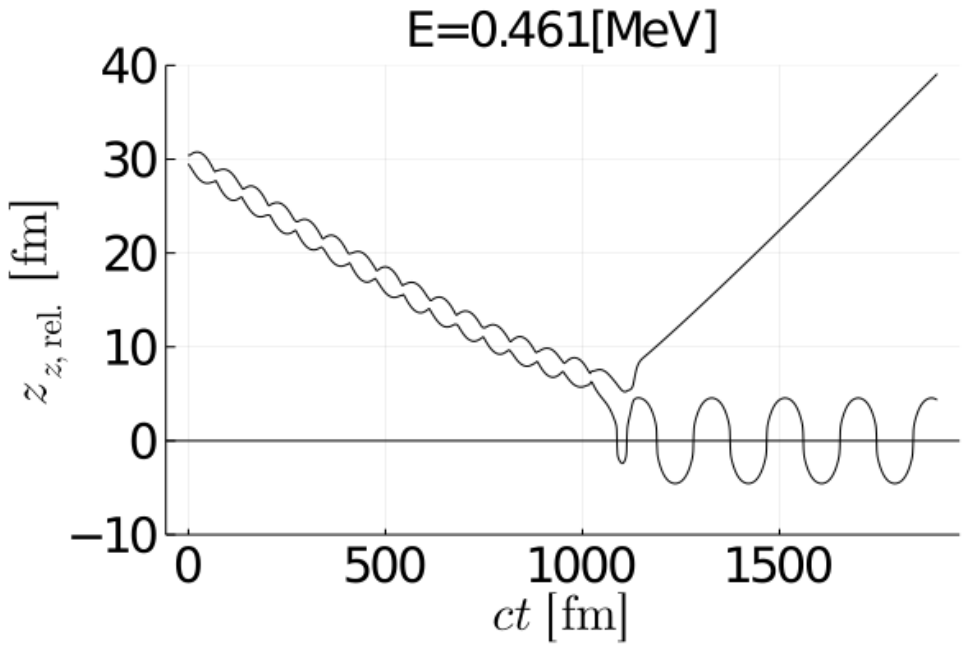

Figure 4.19: Same as Fig. 4.18, but the Slater determinants are time-evolved by TDGCM.

Because of this problem, the TDGCM does not always give good results as the number of superimposed Slater determinants is increased. For example, in the calculation for a collision of ^{4}He with and external barrier, we showed the results when nine Slater determinants were used, and confirmed that the results with eleven Slater determinants were similar, but when more Slater determinants were used, the calculation became unstable. Since superposing too many Slater determinants can cause the above problem, and using too few can result in insufficient convergence, it is necessary to determine the appropriate number of Slater determinants for the system of interest before applying TDGCM.

Further extensions

To close this Section, we will mention the extension of TDGCM. The first possible extension from the present calculation is to reduce the number of approximations. We used five approximations as described above, but by reducing the number of approximations, we can describe more phenomena more accurately. For example, if we exclude the head-on collision assumption, we can describe collisions with different impact parameters and define fusion cross sections in collisions. In another example, if the Gaussian cen-

ter z of the nucleons inside ^{4}He can be moved independently, it would be possible to effectively incorporate the effect of internal excitations. It should also be possible to describe nucleon transfer reactions. In principle, it is also possible to develop spin and isospin wave functions and Gaussian widths in time, or to use single-particle wave functions, which are not limited to Gaussian functions, and these may also contribute to the description of internal excitations. On the other hand, if the number of approximations is reduced and the number of degrees of freedom of the trial function is increased, the above-mentioned problem of computational cost arises, so how much approximations can be reduced in a realistic computational time will be a major issue in the future.

Another direction of extension is to apply it to heavy nuclei. Although only ^{4}He was used in this study, the TDGCM can in principle handle medium to very heavy nuclei. However, the problem here is also the computational cost, since, unlike the case of ^{4}He, one cannot use the approximation to keep the same z for all the nucleons, and the computational cost increases as the number of nucleons increases.pre Also, the number of Slater determinants to be superposed is unknown when the number of nucleons increases.

Chapter 5

Conclusion

In this thesis, we have aimed to develop a microscopic theory that can describe nuclear fusions, especially at low energies. For this purpose, we have investigated the Time-Dependent Generator Coordinate Method (TDGCM), which describes the dynamics of nuclei by a trial function consisting of a time-dependent Slater determinant superposed with time-dependent weights. In this study, we develop a new version of TDGCM based on the Reinhard's simplified TDGCM by incorporating the correlation between Slater determinants. Our TDGCM is a framework that can describe the tunneling effect as well as the internal excitation, which is considered to be impossible to describe in simplified TDGCM. Although TDGCM is expected to be a good method, the computational cost is still expected to be high for realistic calculations. Therefore, we used the approximation that the single-particle wave functions of the Slater determinant are Gaussian with a common fixed width to reduce the computational cost.

After constructing our TDGCM in this way, we tested the method by applying it to three simple systems with ^{4}He. To this end, we assumed that the spin and isospin wave functions are fixed, and the Gaussian centers of the four single-particle wave functions in ^{4}He are assumed to coincide. With this assumption, the Slater determinant representing ^{4}He is characterized by a single Gaussian center z. In order to test whether the TDGCM can describe the quantum tunneling of the Coulomb barrier, which is necessary to describe fusion in the sub-barrier region, we first applied the TDGCM with two Slater determinants to a system of one-dimensional He+He collisions. The interactions used were the zero-range three-body repulsion, the folding Gauss attraction, and the Coulomb interaction for 1D. In this case, the two ^{4}He were assumed to move symmetrically about $x = 0$, for which one ^{4}He has a Gaussian center z and the other has a Gaussian center $-z$. As a result, it was confirmed that the ^{4}He wave function partially penetrates the

barrier in the TDGCM even at collision energies below the barrier. The quantum tunneling phenomenon can thus be qualitatively described. We also found that the TDGCM expresses the barrier penetration, which cannot be expressed by the TDHF, by exchanging the energy between superposed Slater determinants.

Next, in order to calculate the tunneling probability in more details, we applied the TDGCM to a system in which ^{4}He collides with an external barrier in one dimension. In this calculation, the interaction between nucleons is not considered, and only a Gaussian external barrier exists. In this application, nine Slater determinants were superposed to study the energy dependence of the tunneling probability. The same calculations were performed for five, nine, and eleven Slater determinants, and it is confirmed that the calculations converge at nine Slater determinants. Here, the initial Slater determinant was changed to vary the collision energy, and the same Slater determinant was time-evolved with TDGCM or independent AMD. As a result, we obtained discrete barrier penetration probabilities in the independent AMD calculation and smooth barrier penetration probabilities in the TDGCM. This smoothness can be attributed to the time variation of the weights f. In addition, compared with the transmission probability obtained by the AMD calculation, the transmission probability in TDGCM is larger at energies below the barrier, and this increase can be regarded as a description of quantum tunneling. Although the choice of the Slater determinant to represent the same initial wave function is arbitrary in TDGCM, the results are almost the same depending on the choice of the determinant, as confirmed by three samples of Slater determinants.

Finally, as a first step toward more realistic calculations, we applied the TDGCM to colliding of two ^{4}He particles in three dimensions. Although this calculation assumes head-on collision and the degrees of freedom for ^{4}He motion are effectively one-dimensional, this calculation works as an example of three-dimensional calculation. The resulting trajectories show the same behavior as in one-dimensional ^{4}He+^{4}He collisions, indicating that the TDGCM can work in three dimensions.

We here summarizes the significance of our TDGCM in the field of nuclear reactions. Methods based on the mean-field approximation, such as TDHF, which have been widely used for microscopic calculations of nuclear reactions, have the advantage of automatically incorporating the effects of internal excitations, but they underestimate the quantum fluctuations that should be present, and in principle cannot describe the quantum tunneling effect. Several methods beyond TDHF have been developed, such as the simplified TDGCM introduced in Chap. 2, which can recover quantum fluctuations, and TDHW, which ignores the internal excitations but describes

a tunneling phenomenon. On the other hand, a method that automatically included the effect of internal excitations during the nuclear reaction while also describing the tunneling effect has not yet been established, and such a method is necessary for describing low-energy nuclear fusion. Therefore, we have developed a TDGCM that can describe both internal excitations and tunneling effects simultaneously. This method is effective for fusion reactions at low energies, especially below the barrier, and possible applications include nucleosynthesis in stellar interiors and supernovae. In addition, since TDGCM is a microscopic method and no empirical input is necessary, it may provide a useful method in unknown regions where it is difficult to perform experiments, such as reactions in neutron-rich or superheavy nuclei.

In this study, we have constructed the basis of the theory and investigated the ability of the method by applying it to simple systems There will be many important applications in future where this theory can be applied. This study provides an important first step towards such goal.

As future works, we should first see how well the TDGCM takes into account internal excitations. In the present calculations, we have focused only on the description of the tunneling effect and made some approximations, so that internal excitations cannot occur in the calculations. In particular, we should first remove the approximation that makes the position of nucleons in ^{4}He the same, and then include the internal excitations of nuclei. The application of the TDGCM to heavier nuclei also remains to be done. The next target is ^{4}He+^{12}C [104], for which calculations can be compared with experiments.

Bibliography

[1] A. S. Umar, V. E. Oberacker, J. A. Maruhn, Neutron transfer dynamics and doorway to fusion in time-dependent Hartree-Fock theory. Euro. Phys. J. A. **37**, 245 (2008).

[2] Y. Iwata, T. Otsuka, J. A. Maruhn, N. Itagaki, Suppression of charge equilibration leading to the synthesis of exotic nuclei, Phys. Rev. Lett. **104**, 252501 (2010).

[3] M. Evers, M. Dasgupta, D. J. Hinde, D. H. Luong, R. Rafiei, R. du Rietz, et al, Cluster transfer in the reaction 16O+208Pb at energies well below the fusion barrier: a possible doorway to energy dissipation, Phys. Rev. C. **84**, 054614 (2011).

[4] A. S. Umar, C. Simenel, W. Ye, Transport properties of isospin asymmetric nuclear matter using the time-dependent Hartree-Fock method, Phys. Rev. C. **96**, 024625 (2017).

[5] C. Golabek, C. Simenel, Collision dynamics of two 238U atomic nuclei, Phys. Rev. Lett. **103**, 042701 (2009).

[6] D. J. Kedziora, C. Simenel, New inverse quasifission mechanism to produce neutron-rich transfermium nuclei, Phys. Rev. C. **81**, 044613 (2010).

[7] C. Simenel, D. J. Hinde, R. du Rietz, M. Dasgupta, M. Evers, C. J. Lin, et al, Influence of entrance-channel magicity and isospin on quasi-fission, Phys. Lett. B **710**, 607 (2012).

[8] A. Wakhle, C. Simenel, D. J. Hinde, M. Dasgupta, M. Evers, D. H. Luong, et al, Interplay between quantum shells and orientation in quasifission, Phys. Rev. Lett. **113**, 182502 (2014).

[9] S. Simenel, and A.S. Umar, Formation and dynamics of fission fragments, Phys. Rev. C **89**, 031601(R) (2014)

[10] G.Scamps, C.Simenel , and D. Lacroix, Superfluid dynamics of 258Fm fission, Phys. Rev. C. **92**, 011602(R) (2015).

[11] Y. Tanimura, D. Lacroix, and G. Scamps, Collective aspects deduced from time-dependent microscopic mean-field with pairing: application to the fission process, Phys. Rev. C. **92**, 034601 (2015).

[12] A. S. Umar, V. E. Oberacker, Heavy-ion interaction potential deduced from density-constrained time-dependent Hartree-Fock calculation, Phys. Rev. C. **74**, 021601(R) (2006).

[13] A. S. Umar, V. E. Oberacker, J. A. Maruhn, P.-G. Reinhard, Microscopic calculation of precompound excitation energies for heavy-ion collisions, Phys. Rev. C. **80**, 041601(R) (2009).

[14] A. S. Umar, V. E. Oberacker, J. A. Maruhn, P.-G. Reinhard, Entrance channel dynamics of hot and cold fusion reactions leading to superheavy elements, Phys. Rev. C. **81**, 064607 (2010).

[15] V. E. Oberacker, A. S. Umar, J. A. Maruhn, P.-G. Reinhard, Microscopic study of the 132, 124Sn+96Zr reactions: dynamic excitation energy, energy-dependent heavy-ion potential, and capture cross section, Phys. Rev. C. **82**, 034603 (2010).

[16] A. S. Umar, V. E. Oberacker, J. A. Maruhn, P.-G. Reinhard, Microscopic composition of ion-ion interaction potentials, Phys. Rev. C. **85**, 017602 (2012).

[17] V. E. Oberacker, A. S. Umar, J. A. Maruhn, P.-G. Reinhard, Dynamic microscopic study of pre-equilibrium giant resonance excitation and fusion in the reactions 132Sn+48Ca and 124Sn+40Ca, Phys. Rev. C. **85**, 034609 (2012).

[18] M. V. Borunov, P. N. Nadtochy, G. D. Adeev, Nuclear scission and fission-fragment kinetic-energydistribution: Study within three-dimensional Langevindynamics, Nucl. Phys. A **799**, 56-83 (2008).

[19] A. Zdeb, A. Dobrowolski, and M. Warda, Fission dynamics of ^{252}Cf, Phys. Rev. C **95**, 054608 (2017).

[20] D. Regnier, N. Dubray, N. Schunck, and M. Verrière, Fission fragment charge and mass distributions in ^{238}Pu(n, f) in the adiabatic nuclear energy density functional theory, Phys. Rev. C **93**, 054611 (2016).

[21] P.-G. Reinhard, R. Y. Cusson, and K. Goeke, Time evolution of coherent ground-state correlations and the TDHF approach, Nuclear Physics A **398**, 141 (1983).

[22] N. Hasegawa, K. Hagino, Y. Tanimura, Time-dependent generator coordinate method for many-particle tunneling, Phys. Lett. B **808**, 135693 (2020).

[23] K. Sekizawa, K. Yabana, Time-dependent Hartree-Fock calculations for multinucleon transfer and quasifission processes in the ^{64}Ni+^{238}U reaction, Phys. Rev. C **93**, 054616 (2016).

[24] K. Sekizawa, Microscopic description of production cross sections including deexcitation effects, Phys. Rev. C **96**, 014615 (2017).

[25] E. M. Kozulin, G. N. Knyazheva, I. M. Itkis, M. G. Itkis, A. A. Bogachev, L. Krupa, et al, Investigation of the reaction ^{64}Ni+^{238}U being an option of synthesizing element 120, Phys. Lett. B **686**, 227 (2010).

[26] C. R. Morton, A. C. Berriman, M. Dasgupta, D. J. Hinde, J. O. Newton, K. Hagino, I. J. Thompson, Coupled-channels analysis of the 16O+208Pb fusion barrier distribution, Phys. Rev. C **60**, 044608 (1999).

[27] R. H. Cyburt, B. D. Fields, K. A. Olive, and T. H. Yeh, Big bang nucleosynthesis: Present status, Rev. Mod. Phys. **88**, 015004 (2016).

[28] K. Hebeler, J.D. Holt, J. Menéndez, and A. Schwenk, Nuclear Forces and Their Impact on Neutron-Rich Nuclei and Neutron-Rich Matter, Ann. Rev. Nucl. Part. Sci. 65:457-484 (2015).

[29] C. A. Bertulani, L. F. Canto, M. S. Hussein, The structure and reactions of neutron-rich nuclei, Phys. Rep. 226, 6, 281-376 (1993).

[30] B. A. Loiseau, Y. Nogami, C.K.Ross, Nucleon-nucleon correlation and two-pion-exchange three-body force in nuclear matter, Nucl. Phys. A 165, 3, 19, 601-624 (1971).

[31] K. Sekiguchi, H. Sakai, H. Witała, W. Glöckle, J. Golak, M. Hatano, H. Kamada, H. Kato, Y. Maeda, J. Nishikawa, A. Nogga, T. Ohnishi, H. Okamura, N. Sakamoto, S. Sakoda, Y. Satou, K. Suda, A. Tamii, T. Uesaka, T. Wakasa, and K. Yako, Complete set of precise deuteron analyzing powers at intermediate energies: Comparison with modern nuclear force predictions, Phys. Rev. C **65**, 034003 (2002)

[32] R. Machleidt, F. Sammarruca, and Y. Song, Nonlocal nature of the nuclear force and its impact on nuclear structure, Phys. Rev. C **53**, R1483(R) (1996).

[33] S. Aoki, T. Hatsuda and N Ishii, The nuclear force from Monte Carlo simulations of lattice quantum chromodynamics, Comput. Sci. Discov. 1, 015009 (2008).

[34] W. D. Myers and W.J. Swiatecki, The nuclear droplet model for arbitrary shapes, Ann. Phys. **84**, 1-2, 186-210 (1974).

[35] K. Hagino, A. Vitturi, C. H. Dasso, and S. M. Lenzi, Role of breakup processes in fusion enhancement of drip-line nuclei at energies below the Coulomb barrier, Phys. Rev. C **61**, 037602 (2000)

[36] T. Tamura, Analyses of the Scattering of Nuclear Particles by Collective Nuclei in Terms of the Coupled-Channel Calculation, Rev. Mod. Phys. **37**, 679 (1965)

[37] C. Simenel, Nuclear quantum many-body dynamics, Euro. Phys. J. A**48**, 152 (2012).

[38] P. Ring and P. Schuck, *The Nuclear Many Body Problem* (Springer-Verlag, New York, 1980).

[39] P. Bonche, S. Koonin, and J.W. Negele, One-dimensional nuclear dynamics in the time-dependent Hartree-Fock approximation, Phys. Rev. C**13**, 1226 (1976).

[40] J.W. Negele, The mean-field theory of nuclear structure and dynamics, Rev. Mod. Phys. **54**, 913 (1982).

[41] T. Nakatsukasa, K. Matsuyanagi, M. Matsuo, and K. Yabana, Time-dependent density-functional description of nuclear dynamics, Rev. Mode. Phys. **88**, 045004 (2016).

[42] A.K. Dhar, B.S. Nilsson, K.T.R. Davies, and S.E. Koonin, Time-dependent Hartree-Fock study of ^{136}Xe+ ^{209}Bi collisions, Nucl. Phys. **A364**, 105 (1981).

[43] J.A. Maruhn, P.-G. Reinhard, S.D. Stevenson, and A.S. Umar, The TDHF code Sky3D, Comp. Phys. Comm. **185**, 2195 (2014).

[44] A.S. Umar and V.E. Oberacker, Time-dependent HF approach to SHE dynamics, Nucl. Phys. **A944**, 238 (2015).

[45] C. Golabek and C. Simenel, Collision Dynamics of Two ^{238}U Atomic Nuclei, Phys. Rev. Lett. **103**, 042701 (2009).

[46] K. Sekizawa and K. Yabana, Time-dependent Hartree-Fock calculations for multinucleon transfer processes in ^{40,48}Ca+^{124}Sn, ^{40}Ca+^{208}Pb, and ^{58}Ni+^{208}Pb reactions, Phys. Rev. C**88**, 014614 (2013).

[47] K. Sekizawa and K. Yabana, Time-dependent Hartree-Fock calculations for multinucleon transfer and quasifission processes in the ^{64}Ni+^{238}U reaction, Phys. Rev. C**93**, 054616 (2016).

[48] K. Washiyama and D. Lacroix, Energy dependence of the nucleus-nucleus potential close to the Coulomb barrier, Phys. Rev. C**78**, 024610 (2008).

[49] G. Scamps and D. Lacroix, Effect of pairing on one-and two-nucleon transfer below the Coulomb barrier: A time-dependent microscopic description, Phys. Rev. C**87**, 014605 (2013).

[50] A. Bulgac, P. Magierski, K.J. Roche, and I. Stetcu, Induced Fission of ^{240}Pu within a Real-Time Microscopic Framework, Phys. Rev. Lett. **116**, 122504 (2016).

[51] C. H. Patterson, Photoabsorption spectra of small Na clusters: TDHF and BSE versus CI and experiment, Phys. Rev. Materials **3**, 043804 (2019).

[52] Y. Tanimura, D. Lacroix, and S. Ayik, Microscopic Phase-Space Exploration Modeling of Spontaneous Fission, Phys. Rev. Lett. **118**, 152501 (2017).

[53] C.-Y. Wong and H.H.K. Tang, Extended time-dependent Hartree-Fock approximation with particle collisions, Phys. Rev. Lett. **40**, 1070 (1978).

[54] S.J. Wang and W. Cassing, Explicit treatment of N-body correlations within a density-matrix formalism, Ann. Phys. (N.Y.) **159**, 328 (1985).

[55] M. Gong and M. Tohyama, Application of a time-dependent density-matrix formalism, Z. Phys. **A335**, 153 (1990).

[56] S. Ayik, Nuclear quantum many-body dynamics, Phys. Lett. B **658**, 174 (2008).

[57] D. Lacroix and S. Ayik, Stochastic quantum dynamics beyond mean field, Euro. Phys. J. A**50**, 95 (2014).

[58] M. Colonna and P.h. Chomaz, Unstable infinite nuclear matter in stochastic mean field approach, Phys. Rev. C **49**, 1908 (1994).

[59] P.-G. Reinhard and E. Suraud, Stochastic TDHF and the Boltzman-Langevin equation, Ann. of Phys. (N.Y.) **216**, 98 (1992).

[60] L. Lacombe, P.-G. Reinhard, P.M. Dinh, and E. Suraud, A collisional extension of time-dependent Hartree–Fock, J. of Phys. B**49**, 245101 (2016).

[61] P. Grange, H.A. Weidenmüller, and G. Wolschin, Beyond the tdhf: A collision term from a random-matrix model, Ann. of Phys. (N.Y.) **136**, 190 (1981).

[62] H. Reinhardt, R. Balian, and Y. Alhassid, ended time-dependent mean-field theories from the maximum-entropy principle, Nucl. Phys. **A422**, 349 (1984).

[63] R. Balian and M. Veneroni, Fluctuations in a time-dependent mean-field approach, Phys. Lett. B**136**, 301 (1984).

[64] A. Donoso and C.C. Martens, Quantum tunneling using entangled classical trajectories, Phys. Rev. Lett. **87**, 223202 (2001).

[65] A. Wang, Y. Zheng, C. C. Martens, and W. Ren, Quantum tunneling dynamics using entangled trajectories: general potentials, Phys. Chem. Chem. Phys. **11**, 1588 (2009).

[66] L. Wang, C.C. Martens, and Y. Zheng, Entangled trajectory molecular dynamics in multidimensional systems: Two-dimensional quantum tunneling through the Eckart barrier, J. of Chem. Phys. **137**, 034113 (2012).

[67] F. Xu, L. Zhang, L. Jiang, L. Bao, and H. Meng, Quantum tunneling effect in entanglement dynamics, Int. J. Quant. Chem. **116**, 7 (2016).

[68] E. Orestes, K. Capelle, A.B. da Silva, and C.A. Ullrich, Generator coordinate method in time-dependent density-functional theory: Memory made simple, J. Chem. Phys. **127**, 124101 (2007).

[69] D. Regnier and D. Lacroix, Microscopic description of pair transfer between two superfluid Fermi systems. II. Quantum mixing of time-dependent Hartree-Fock-Bogolyubov trajectories, Phys. Rev. C **99**, 064615 (2019).

[70] R. Bernard, H. Goutte, D. Gogny, and W. Younes, Microscopic and nonadiabatic Schrödinger equation derived from the generator coordinate method based on zero-and two-quasiparticle states, Phys. Rev. C **84**, 044308 (2011).

[71] H. Goutte, J. F. Berger, P. Casoli, and D. Gogny, Microscopic approach of fission dynamics applied to fragment kinetic energy and mass distributions in ^{238}U, Phys. Rev. C **71**, 024316 (2005).

[72] H. Tao, J. Zhao, Z. P. Li, T. Nikšić, and D. Vretenar, Microscopic study of induced fission dynamics of ^{226}Th with covariant energy density functionals, Phys. Rev. C **96**, 024319 (2017).

[73] K. Hagino and N. Takigawa, Subbarrier fusion reactions and many-particle quantum tunneling, Prog. Theo. Phys. **128**, 1061 (2012).

[74] Y. Kanada-En'yo, M. Kimura, and A. Ono, Antisymmetrized molecular dynamics and its applications to cluster phenomena, Prog. Theo. Exp. Phys. **2012**, 01A202 (2012).

[75] A. Ono, H. Horiuchi, T. Maruyama, and A. Ohnishi, Antisymmetrized version of molecular dynamics with two-nucleon collisions and its application to heavy ion reactions, Prog. Theor. Phys. **87**, 1185 (1992).

[76] M.S. Pindzola, D.C. Griffin, and C. Bottcher, Validity of time-dependent Hartree-Fock theory for The multiphoton ionization of atoms, Phys. Rev. Lett. **66**, 2305 (1991).

[77] R. Grobe and J.H. Eberly, Photoelectron spectra for a two-electron system in a strong laser field, Phys. Rev. Lett. **68**, 2905 (1992).

[78] R. Grobe and J.H. Eberly, One-dimensional model of a negative ion and its interaction with laser fields, Phys. Rev. A**48**, 4664 (1993).

[79] M. Lein, E.K.U. Gross, and V. Engel, Intense-field double ionization of helium: identifying the mechanism, Phys. Rev. Lett. **85**, 4707 (2000).

[80] T. Maruyama, T. Oishi, K. Hagino, and H. Sagawa, Time-dependent approach to many-particle tunneling in one dimension, Phys. Rev. C**86**, 044301 (2012).

[81] H. Flocard and D. Vautherin, Generator coordinate calculations of giant resonances with the Skyrme interaction, Nucl. Phys. **A264**, 197 (1976).

[82] J. Richert, D.M. Brink, and H.W. Weidenmüller, Numerical solution of one-dimensional TDHF equations without and with a collision term, Phys. Lett. **87B**, 6 (1979).

[83] H. Feldmeier, and J. Schnack, Molecular dynamics for fermions, Rev. Mod. Phys. **72**, 655 (2000)

[84] A.K. Kerman, and S.E. Koonin, Hamiltonian formulation of time-dependent variational principles for the many-body system, Ann. Phys. **100**, 332-358 (1976)

[85] P. Kramer, and M. Saraceno, Geometry of the Time-Dependent Variational Principle in Quantum Mechanics, Lecture Notes in Physics, Springer, **140**, 3-14 (1981)

[86] S. Drożdż, M, Ploszajczak, and E. Caurier, Variational approach to the Schrödinger dynamics in the Klauder's continuous representations, Ann. Phys., **171**, 1, 108-131 (1986)

[87] J. Broeckhove, L. Lathouwers, E. Kesteloot, and P.V. Leuven, On the equivalence of time-dependent variational principles, Chem. Phys. Lett, **149**, 5-6, 547-550 (1988)

[88] E. Gerjuoy,A.R.P. Rau, and L. Spruch, A unified formulation of the construction of variational principles, Rev. Mod. Phys. **55**, 725 (1983)

[89] R. Balian, and M. Veneroni, Static and dynamic variational principles for expectation values of observables, Ann. Phys., **187**, 1, 29-78 (1988)

[90] P.A.M. Dirac, Note on exchange phenomena in the thomas atom. Proc Camb Philos Soc. **26** 376(1930)

[91] P. Bonche, S. Koonin, and J. W. Negele, One-dimensional nuclear dynamics in the time-dependent Hartree-Fock approximation, Phys. Rev. C **13**, 1226 (1976)

[92] C. Gardiner and P. Zoller, Quantum Noise: A Handbook of Markovian and non-Markovian Quantum Stochastic Methods with Applications to Quantum Optics (Springer Science and Business Media, Berlin-Heidelberg, 2004)

[93] A. Sinatra, C. Lobo, and Y. Castin, The truncated Wigner method for Bose-condensed gases: limits of validity and applications, J. Phys. B **35**, 3599 (2002)

[94] F. Gelis and B. Schenke, Initial-state quantum fluctuations in the little bang, Annu. Rev. Nucl. Part. Sci. **66**, 73 (2016).

[95] A. S. Umar, J. A. Maruhn, N. Itagaki, V. E. Oberacker, Microscopic study of the triple- reaction, Phys. Rev. Lett. **104**, 212503 (2010).

[96] T. Ichikawa, K. Matsuyanagi, J. A. Maruhn, N. Itagaki, Pure collective precession motion of a high-spin torus isomer, Phys. Rev. C. **89**, 011305(R) (2014).

[97] T. Ichikawa, K. Matsuyanagi, J. A. Maruhn, N. Itagaki, High-spin torus isomers and their precession motions, Phys. Rev. C. **90**, 034314 (2014).

[98] T. Cooper, W. Bertozzi, J. Heisemberg, S. Kowalski, W. Turchinetz, C. Williamson, L. Cardman, S. Fivozinsky, J. Lightbody, Jr., and S. Penner, Shapes of deformed nuclei as determined by electron scattering: Sm152, Sm154, Er166, Yb176, Th232, and U238, Phys. Rev. C. **13**, 1083 (1976)

[99] A. Tohsaki, H. Horiuchi, P. Schuck, and G. Röpke, Alpha Cluster Condensation in ^{12}C and ^{16}O, Phys. Rev. Lett. **87**, 192501 (2001)

[100] B. Buck, A. C. Merchant, and S. M. Perez, Alpha-cluster structure in ^{212}Po, Phys. Rev. Lett. **72**, 1326 (1994)

[101] K. Sekizawa, TDHF Theory and Its Extensions for the Multinucleon Transfer Reaction: A Mini Review, Front. Phys. 7:20 (2019)

[102] L. Corradi, A. M. Stefanini, C. J. Lin, S. Beghini, G. Montagnoli, F. Scarlassara, et al., Multinucleon transfer processes in ^{64}Ni+^{238}U, Phys. Rev. C **59**, 261 (1999).

[103] A. B. Volkov, Equilibrium deformation calculations of the ground state energies of 1p shell nuclei, Nucl. Phys. **74**, 33-58 (1965)

[104] K. Sagara, K Fujita, H. Yamaguchi, K. Hamamoto, Y. Narikiyo, N. Tao, and T. Ban, Direct Measurement of ^{12}C + ^{4}He Fusion Cross Section Down to E_{cm} =1 MeV and Prospects JPS Conf. Proc. 14, 010404 (2017).